INNOVATION FOREVER
Open Access

Innovation Discovery
ISSN 2959-5150 (Online)

Review

Next-Generation Manufacturing of Shape Memory Alloys via Laser-Based Additive Processes: Enabling 4D-Printed Smart Structures

Peyman Asghartabar Kashi[1,2], **Mahdi Didari**[3], **Mahdiyar Shahbazi**[2*]

[1]*Faculty of Biosystem, College of Agricultural and Natural Resources, Tehran University, Karaj, Iran*
[2]*Institute of Technology, University of Natural Resources and Life Sciences (BOKU), Vienna, Austria*
[3]*Department of Nutritional Sciences, University of Vienna, Vienna, Austri*

[*]***Correspondence to: Mahdiyar Shahbazi,*** *Institute of Technology, University of Natural Resources and Life Sciences (BOKU), Muthgasse 18, 1190 Vienna, Austria; Email: shahbazim00@yahoo.com*

Abstract

Shape memory alloys (SMAs) are transformative materials renowned for their ability to reversibly change shape in response to thermal and mechanical stimuli. While nitinol (NiTi) remains the most extensively studied SMA, a growing portfolio of alternative systems, particularly copper-based alloys, offer compelling advantages in cost, durability, and functional versatility. These materials are increasingly vital in demanding environments requiring high performance, corrosion resistance, and tailored thermomechanical behavior. Recent breakthroughs in additive manufacturing, especially laser powder bed fusion (LPBF), have revolutionized the fabrication of complex SMA components, enabling unprecedented microstructural control, intricate architectures, and customized properties. This review synthesizes cutting-edge research on LPBF processing of diverse SMA systems, emphasizing how process parameters influence phase transformations, microstructural evolution, defect formation, and functional stability. It explores innovative structural designs, such as lattice and auxetic configurations, that unlock new levels of performance in biomedical devices, aerospace actuators, and energy absorption systems. Despite significant progress, challenges such as residual stresses, material homogeneity, and scalability continue to hinder widespread deployment. This review highlights promising avenues for future research: optimizing alloy compositions, refining processing techniques, and expanding application horizons. By advancing our understanding of microstructure-property relationships, these efforts aim to unlock the full potential of both traditional and emerging SMAs across a broad spectrum of industries.

Keywords: shape memory alloys, laser powder bed fusion, selective laser melting, wire-based deposition printing, electron beam melting, smart structures

Received: December 29, 2025
Revised: March 30, 2026
Accepted: June 2, 2026
Published: June 30, 2026

Citation: Kashi PA, Didari M, Shahbazi M. Next-Generation Manufacturing of Shape Memory Alloys via Laser-Based Additive Processes: Enabling 4D-Printed Smart Structures. *Innov Discov*, 2026; 3(2): 10.

1 INTRODUCTION

Shape memory alloys (SMAs) constitute a unique class of smart materials characterized by their intrinsic ability to undergo reversible deformation and recover their original shape upon exposure to external stimuli such as temperature or mechanical load[1-3]. This remarkable behavior is primarily driven by a reversible martensitic transformation between high-symmetry austenite and low-symmetry martensite phases[4,5], which confers functionalities such as the shape memory effect (SME) and superelasticity (SE)[6-10]. These properties have catalyzed extensive research and diverse applications across actuators[11] aerospace[12], biomedical[13], civil[14], and energy sectors[15].

While nickel-titanium alloy (NiTi or Nitinol) remains the flagship SMA owing to its outstanding combination of SME, SE, corrosion resistance, and biocompatibility, the broader landscape encompasses various other alloy systems, each with distinct microstructural features and functional profiles[6-8]. Copper-based SMAs, including Copper-Zinc-Aluminum (Cu-Zn-Al), Copper-Aluminum-Nickel (Cu-Al-Ni), and Copper-Tin (Cu-Sn), are valued for their cost-effectiveness, high thermal conductivity,

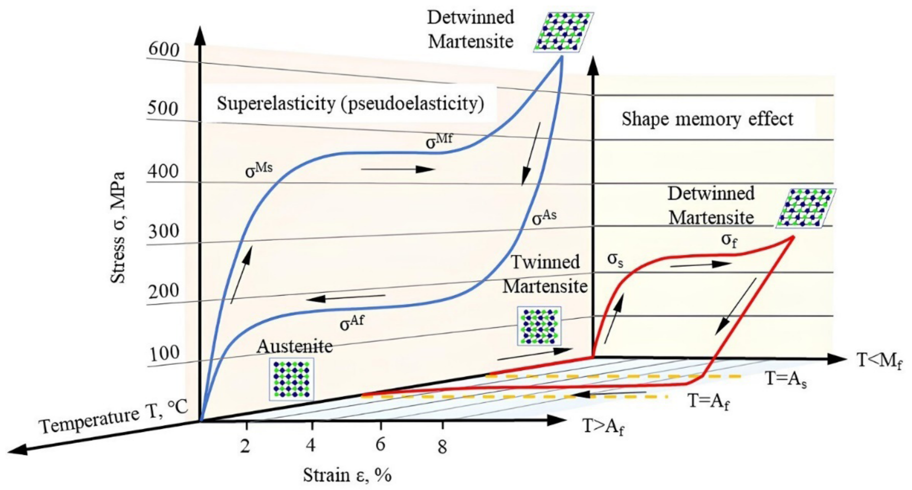

Figure 1. Diagram Illustrating the Mechanisms behind the Shape Memory Phenomenon and Superelastic Response in Shape Memory Materials. Reprinted with Permission from Ref.[23].

and rapid response, although their applications are often limited by poor corrosion resistance and thermal stability[8-10]. Iron-based SMAs, such as Iron-Manganese-Silicon (Fe-Mn-Si) and Iron-Palladium (Fe-Pd), offer advantages like high mechanical strength and environmental stability, making them suitable for structural and actuation roles. While NiTi remains the gold standard for implantable devices due to its proven biocompatibility, Cu-based SMAs are primarily restricted to non-implantable or short-term biomedical applications where cytotoxicity risks can be mitigated[16,17]. Their advantages, such as lower cost, rapid response, and antimicrobial properties, are leveraged in scenarios minimizing direct tissue exposure (e.g., surface coatings, external prosthetics, or sterilizable tools). Recent studies suggest that surface modifications and alloy design can further reduce Cu ion leaching, enabling safer utilization in controlled environments[18-20].

The functional behavior of SMAs is intricately linked to their microstructure, which is influenced by alloy composition, processing history, and thermal-mechanical treatments. For NiTi, the phase transformation involves a hysteretic, diffusionless, and thermoelastic transition that can be finely tuned by alloying elements (e.g., Fe, Cu, Hf) and heat treatments to optimize transformation temperatures and fatigue life. However, traditional manufacturing routes, including casting, hot rolling, and powder metallurgy; face limitations in producing complex geometries, microstructural homogeneity, and defect-free surfaces, which are critical for reliable SMA performance.

Conventional fabrication techniques often introduce impurities, induce residual stresses, and result in microstructural heterogeneity, adversely affecting the shape memory properties and mechanical durability[21]. For instance, casting processes can generate macrosegregation and secondary phases like TiC or $Ti_4Ni_2O_x$, which deteriorate functional stability[22]. Powder metallurgy, while offering some microstructural control, often suffers from porosity, poor surface finish, and limited complexity in shape[23] (Figure 1).

The advent of additive manufacturing (AM), particularly LPBF, has revolutionized the fabrication of SMAs by enabling near-net-shape, highly complex, and customized components with unprecedented microstructural control[24,25]. LPBF involves layer-wise melting of metal powders using a high-energy laser beam, allowing rapid solidification rates (up to 10^6K s^{-1}) that produce non-equilibrium microstructures with high supersaturation, metastability, and refined grain structures[26-29]. These microstructural features are pivotal in tailoring the functional properties, such as transformation temperatures, hysteresis, and fatigue life, of SMA components[30,31].

Various AM methods have been investigated for producing SMAs, encompassing a range of techniques such as powder-bed fusion processes like LPBF[32-35], powder-flow-based approaches such as direct energy deposition (DED)[36-40], wire-based deposition methods[41-43], and electron beam melting (EBM)[44,45]. Among these, LPBF has gained prominence specifically for NiTi alloys, primarily due to its superior capacity for precise dimensional control, the ability to produce parts with densities approaching those of traditionally melted ingots when process parameters are optimized, and its versatility in fabricating complex geometries with high free-forming capabilities[46-50]. In contrast, powder-flow and wire deposition techniques generally exhibit more limitations in resolution and the complexity of attainable structures, especially when intricate geometries or porous architectures are required.

While EBM also employs a powder bed as its energy source, it typically operates at higher process temperatures and offers different microstructural characteristics[51-53]. However, matching the quality and surface finish achieved by LPBF remains challenging, and thus, EBM has seen

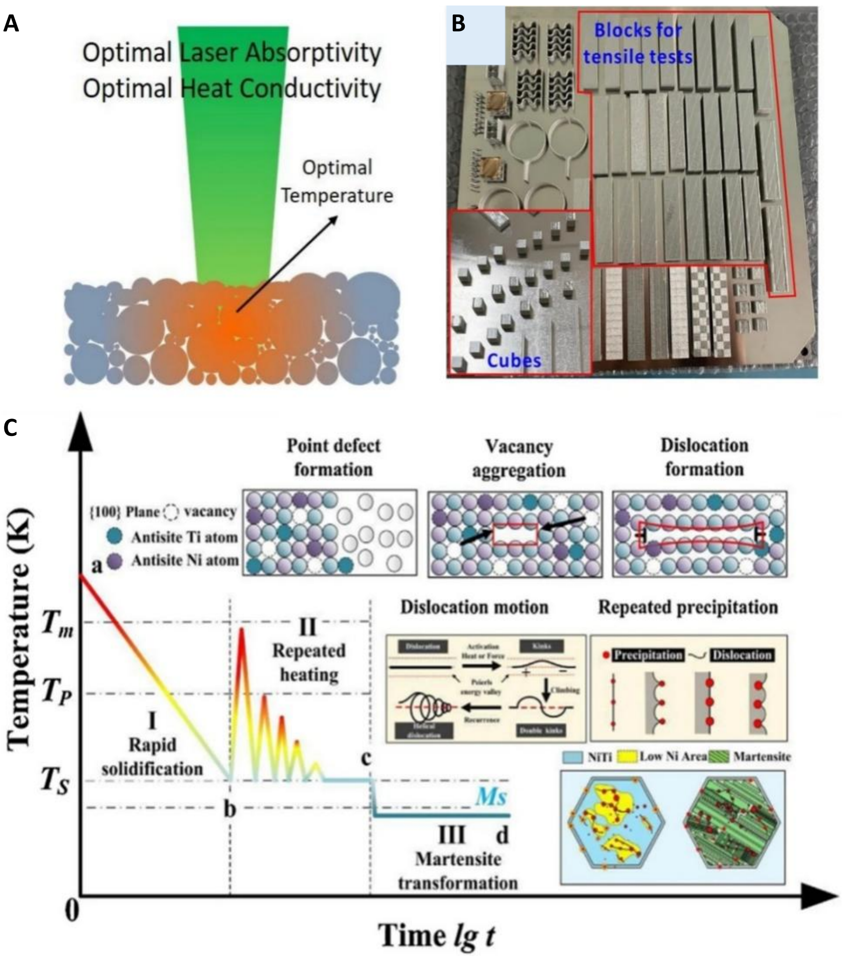

Figure 2. Schematic Overview of SLM Processes and Microstructural Development of NiTi Alloys. (A) Underlying process mechanism of selective laser melting (SLM) technology. Reprinted with Permission from Ref.[54]. (B) Various intricate NiTi alloy structures fabricated through SLM techniques. Reprinted with Permission from Ref.[55]. (C) Thermal processes and microstructural development during the fabrication of NiTi alloys via SLM. Reprinted with Permission from Ref.[56].

comparatively limited application in the fabrication of NiTi SMAs. The intrinsic requirements for high resolution and precise dimensional accuracy are especially critical when fabricating porous or architected NiTi structures, where any deviation or constraint in the manufacturing process can significantly impact the functional performance and structural integrity[55] (Figure 2).

Research has demonstrated that LPBF processing parameters, such as laser power, scan speed, hatch spacing, layer thickness, and scan strategy, significantly influence the resulting microstructure, residual stresses, and phase distribution[56,57]. For example, optimizing laser parameters can minimize residual stresses and improve phase homogeneity, thereby enhancing functional stability and fatigue performance[58]. Moreover, the rapid cooling rates facilitate the formation of fine martensitic variants[59,60], which can be exploited to tailor transformation hysteresis and shape recovery behavior[61,63]. Beyond NiTi, the application of LPBF has expanded to other SMA systems, including Cu-based and Fe-based alloys. For instance, recent studies have successfully fabricated Cu-Zn-Al and Fe-Mn-Si components, demonstrating that process parameter control can produce microstructures with desirable transformation temperatures and mechanical properties[9,10,64,65]. The ability to produce intricate architectures such as porous lattices, functionally graded structures, and microchannels has opened new horizons in biomedical implants, aerospace actuators, and energy harvesting devices[66]. Research into complex NiTi components produced through wire-based or powder-flow melting techniques remains sparse, partly due to the technical challenges associated with achieving comparable resolution and microstructural control. Consequently, the focus of this chapter will primarily be on NiTi parts manufactured via LPBF, emphasizing its advantages in creating architected structures with high precision and functional reliability.

Furthermore, the integration of in-situ monitoring, heat treatment, and post-process thermomechanical treatments with LPBF can further refine microstructure, reduce residual stresses, and improve fatigue life[67,68]. Advanced computational modeling, including finite element and phase-field simulations, is increasingly employed to predict microstructural evolution, transformation behavior, and mechanical response, guiding process optimization and alloy design.

SMAs are renowned for their intrinsic ability to undergo reversible, stimulus-driven phase transformations that result in shape changes over time, forming the basis of the "fourth dimension" in 4D printing. AM techniques, such as laser-based processes play a pivotal role in harnessing and enhancing these properties. The layer-by-layer fabrication approach enables precise control over microstructure, microvoid distribution, and internal architecture, which are critical factors influencing phase transformation kinetics, response times, and actuation reliability. Moreover, AM allows for the creation of spatially graded and complex internal geometries, facilitating programmable and multi-step shape morphing tailored to specific applications. Post-processing treatments like heat and thermomechanical conditioning further refine phase stability and transformation temperatures, optimizing the dynamic shape memory response. By leveraging the microstructural and architectural versatility offered by AM, researchers can engineer SMA components with customized time-dependent behaviors, unlocking advanced functionalities for applications in soft robotics, biomedical devices, and aerospace deployable systems that require precise control over shape change timing and performance.

While conventional 3D-printed SMAs primarily exhibit static shape memory and superelastic properties, the concept of 4D printing introduces an additional, dynamic dimension, time, allowing structures to undergo autonomous or stimuli-responsive transformations over multiple stages. This "fourth dimension" is realized through the strategic design and engineering of microstructures, complex internal architectures, and multi-material integrations enabled by AM. These capabilities facilitate programmable, staged, and multi-functional shape changes, transforming static SMA components into adaptive systems capable of multi-step actuation and reconfiguration. AM thus provides the essential microstructural control, geometric complexity, and functional integration necessary to unlock this temporal dimension, advancing the development of truly "4D-printed" SMA structures.

Despite these advancements, challenges remain, including controlling residual stresses, managing porosity, and ensuring reproducibility of functional properties across complex geometries[1]. Additionally, the develpment of multicomponent and high-entropy SMAs via LPBF is an emerging frontier, promising alloys with superior performance and multifunctionality[69]. The ongoing evolution of AM technologies, such as directed energy deposition and hybrid manufacturing, further broadens the scope for SMA innovation.

This review consolidates recent progress in the processing, microstructural engineering, and functional optimization of diverse SMAs fabricated via LPBF. It emphasizes the influence of process parameters on microstructure and properties, explores the challenges in industrial translation, and discusses future directions for designing next-generation SMA components with tailored functionalities for demanding applications.

2 LASER-BASED AM TECHNOLOGIES: RESEARCH METHODOLOGY

The evolution of metal AM since the early 1990s has revolutionized the way complex, high-performance components are designed and fabricated[70]. Central to this progress is the ability of metallic materials, primarily in powder or wire form, to be built layer-by-layer into intricate geometries, often surpassing traditional manufacturing techniques in precision and flexibility[71]. The classification of these systems hinges on the type of feedstock and the energy source employed to selectively fuse the material, with laser and electron beams being the predominant sources[72]. Laser-based approaches, including selective laser sintering (SLS), SLM, and direct metal laser sintering (DMLS), are widely used for high-resolution, detailed structures, whereas EBM offers unique microstructural benefits, especially for NiTi alloys[70].

To standardize terminology and operational mechanisms, the industry and scientific community adhere to the International Organization for Standardization/American Society for Testing and Materials 52900:2021 classification, which delineates AM into seven categories: LPBF, DED, sheet lamination, material extrusion, vat photopolymerization, material jetting, and binder jetting. Among these, PBF, which includes techniques like LPBF, SLM and EBM, has gained particular prominence for metallic applications due to its capacity for producing complex, high-precision parts[73,74].

Within the PBF domain, two main processes, EBM and LPBF, have demonstrated notable success in fabricating NiTi SMAs. Research indicates that EBM can produce NiTi components with homogeneous microstructures, minimal contamination, and preserved functional properties such as shape memory and SE[75]. Recent studies[76,77] have confirmed that NiTi structures produced via EBM maintain their characteristic pseudoelastic behavior, often outperforming traditionally manufactured counterparts.

To elucidate the current landscape of research, a rigorous literature review was conducted across multiple electronic databases, principally Web of Science, employing a systematic, multi-stage filtering process. The initial phase involved identifying influential, highly cited publications directly related to AM and NiTi alloys. Through bibliographic snowball sampling, examining references within these foundational papers, additional relevant studies were uncovered, ensuring comprehensive coverage of the field[78].

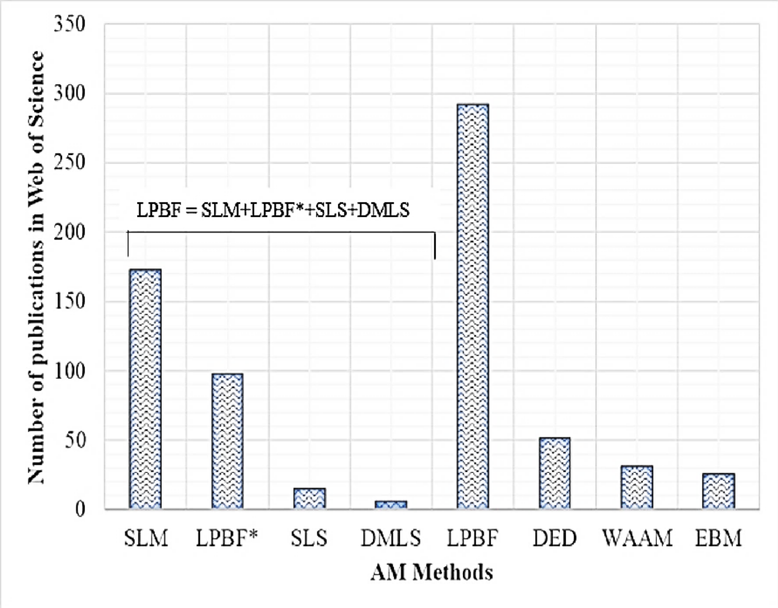

Figure 3. The Distribution of NiTi Alloy Manufacturing Methods Used in AM, Showing the Number of Related Publications in Web of Science; it Groups LPBF, SLM, SLS, and DMLS, with LPBF* Representing Studies where Authors Specifically Use the Term "LPBF" to Describe the Process. Reprinted with Permission from Ref.[79].

The search strategy employed complex Boolean queries combining keywords such as NiTi SMAs, SE, 3D printing, LPBF, and related terms. These were connected via logical operators to maximize retrieval breadth and relevance. The inclusion criteria focused strictly on peer-reviewed articles that documented experimental results, industrial applications, or technological advancements in AM processing of NiTi, excluding non-validated sources such as grey literature or technical reports. This meticulous process culminated in a curated collection of 343 articles, forming the backbone of this review[79]. Figure 3 illustrates the distribution of research publications over recent years, demonstrating a steady increase in scientific interest and technological development in the field. The upward trend depicted in Figure 3 highlights the rapid expansion of studies focusing on AM processes for NiTi alloys, especially in the last five years. It should be noted that SLS and LPBF are both powder-based 3D printing techniques that utilize a laser to process metal or polymer powders. However, they differ significantly in their underlying processes and material characteristics. SLS involves sintering the powder particles, where the laser heats the powder to a temperature below its melting point, causing particles to fuse together without fully melting. This results in parts that are typically less dense and have slightly lower mechanical properties compared to fully melted parts. In contrast, LPBF uses a higher-energy laser to completely melt the powder particles, resulting in a fully dense, solid part with properties comparable to those produced by traditional manufacturing methods. Due to this fundamental difference, sintering versus full melting, LPBF generally produces parts with higher strength, density, and surface finish, making it suitable for applications requiring high precision and mechanical performance.

Furthermore, an analysis of the types of AM methods employed is summarized in Figure 4, which shows the dominance of SLM, a subset of LPBF, in current research efforts. The rising volume of literature dedicated to NiTi fabrication via SLM underscores its significance and potential for industrial applications. Figure 4 captures this growth trajectory, emphasizing the increasing adoption of SLM technology for producing complex, functional NiTi components across biomedical, aerospace, and engineering sectors.

This comprehensive and unbiased synthesis provides a nuanced understanding of the current capabilities, limitations, and future directions for the AM of NiTi SMAs. The integration of systematic literature analysis with cutting-edge manufacturing insights underscores the transformative potential of AM technologies, promising innovative solutions for advanced functional materials. As research continues to evolve, innovations in process optimization and material formulation are poised to unlock new possibilities in biomedical, aerospace, and engineering domains.

3 CHARACTERISTICS OF SMAS

3.1 The Shape Memory Effect

SMAs exhibit remarkable behaviors rooted in their phase transformation characteristics, primarily involving two crystalline states: the high-temperature austenitic phase and the low-temperature martensitic phase. The austenitic phase is distinguished by higher symmetry in its crystal structure, typically adopting a body-centered cubic (BCC) or face-centered cubic (FCC) configuration, whereas the martensitic phase manifests at lower temperatures with reduced symmetry, enabling the

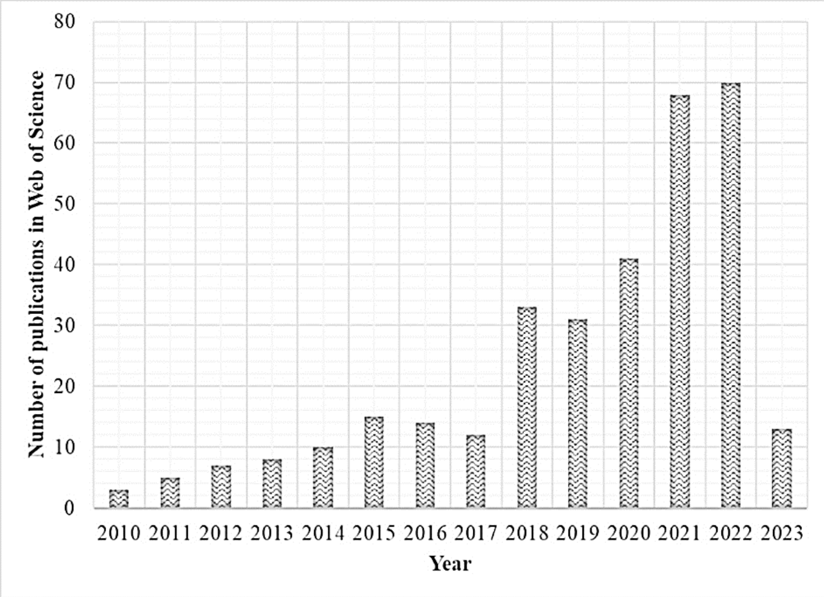

Figure 4. The Yearly Publication Volume of 3D Printing of NiTi Alloy Research Articles Indexed in the Web of Science Database. Reprinted with Permission from Ref.[79].

formation of multiple variants originating from a single parent crystal. This simultaneous presence of parent and transformed phases during the transition is known as the shape memory transformation (SMT), which is mainly driven by Gibbs free energy differences influenced by temperature or applied stress[80].

Unlike typical metals that deform plastically through slip mechanisms, SMAs undergo reversible deformations through atomic rearrangements within the martensitic structure, allowing complete shape recovery. This fundamental difference in crystal structure between austenite and martensite underpins the SME, enabling significant macroscopic shape changes. The phase transformation from austenite to martensite involves a coordinated shear movement of atoms, a solid-state phase change categorized as either thermoelastic or non-thermoelastic. Thermoelastic transformations are characterized by mobile phase interfaces, permitting elastic strain accommodation and reversible behavior, often resulting in twinned martensite structures. Conversely, non-thermoelastic transformations, similar to those in carbon steels, involve immobile interfaces and rely on dislocation mechanisms for strain accommodation, leading to irreversible phase changes that cannot revert spontaneously[81].

The transition between phases occurs over specific temperature ranges defined by Ms (martensite start), Mf (martensite finish), As (austenite start), and Af (austenite finish). These temperatures mark the beginning and completion of phase changes, with hysteresis observed due to energy dissipation during transformation. The SME can be classified into one-way or two-way effects: the one-way SME enables the material to recover its original shape when heated above Af, while the two-way SME allows the material to alternate between two distinct shapes through specialized thermomechanical training.

The typical process of SME can be illustrated through a sequence of stages, often depicted in a cycle:

1. Cooling and Martensitic Formation (1→2): Starting with austenite at a temperature above Af, cooling below Ms and Mf induces the formation of twinned martensite (1→2). This transformation occurs without external stress, with martensitic variants forming in a self-accommodating manner within the parent phase.

2. Stress-Induced Detwinning (2→3): Applying mechanical stress causes the twinned martensite to reorient, a process called detwinning, resulting in inelastic deformation (2→3). This reorientation occurs below Mf and at stresses below the plastic yield limit, producing strains that are not fully recovered upon unloading.

3. Unloading Phase (3→4): Removing the stress leaves the detwinned martensite in a deformed state, with the inelastic strain remaining until the next phase.

4. Heating and Shape Recovery (4→1): Heating the deformed alloy above Af triggers a reverse transformation to austenite, restoring the original shape and fully recovering the inelastic strains. This process is thermally driven and occurs without external stress, resulting in shape recovery due to the phase change[13].

This sequence exemplifies how SMAs utilize phase transformations to enable reversible shape changes, making them highly valuable for diverse applications (Figure 5).

3.2 Superelasticity/Pseudoelasticity in SMAs

Pseudoelasticity, also referred to as SE, is a distinctive characteristic of SMAs that enables the material to

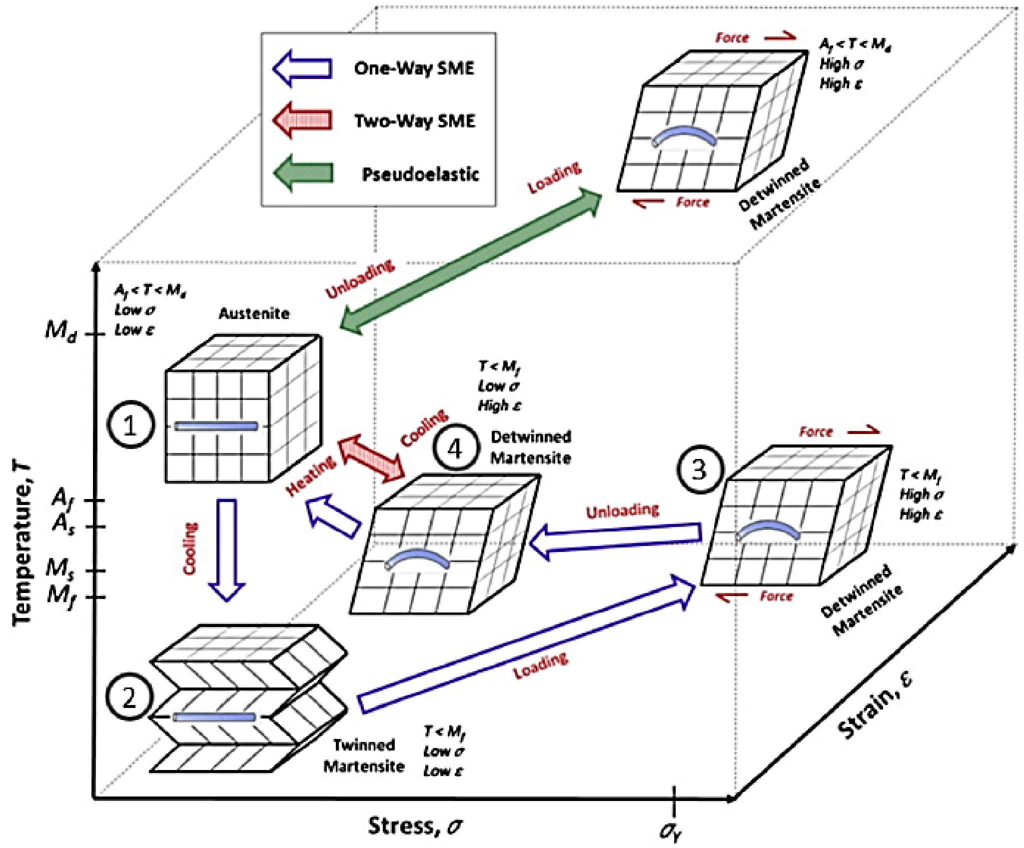

Figure 5. The Transformation Diagram Shows the Phase Changes in SMAs during Thermal Cycles, Highlighting Temperature Ranges, Phase Stability, and the Reversible Nature of PHASES. It helps researchers understand the mechanisms behind shape memory and SE. Reproduced from Ref.[82] with permission.

undergo significant nonlinear deformation and then recover its original shape once the applied stress is removed. This behavior occurs when the temperature is above the austenite finish temperature (Af), typically within a range where the alloy can transition between phases. Specifically, superelasticity is observed only when the temperature exceeds Af; if the temperature falls below this point, stress-induced martensite (SIM) cannot revert back to austenite. Moreover, if the deformation temperature becomes too high, the transformation stress may surpass the yielding strength of materials, leading to permanent plastic deformation. The onset of phase transformation depends on the applied stress level, with higher stresses prompting transformation at elevated temperatures. To broaden the temperature range over which superelasticity can occur, one strategy is to enhance the yielding strength of the alloy, often achieved through processes like work hardening or precipitation hardening.

In contrast to the SME, pseudoelasticity does not require any temperature change. Instead, increasing the applied load causes the alloy to transform from austenite to martensite purely through stress. When the load is removed, the martensite reverts to austenite, allowing the material to recover its original shape. This process results in large, recoverable strains and involves a stress-induced martensitic phase change. For SMAs including copper, the stress-strain response typically exhibits a noticeable hysteresis loop, which highlights their suitability for energy dissipation in damping applications.

4 EXPLORING AM STRATEGIES FOR SMAS

4.1 Fabrication of SMAs Using SLM

4.1.1 NiTi-based Objects

SLM employs a highly focused laser beam as the energy source to fuse metal powders layer by layer, enabling the fabrication of complex, near-net-shape structures with remarkable precision. The process hinges on meticulously controlling the laser's intensity and scanning strategy to locally reach the melting temperature of the powder bed, as illustrated in Figure 2[83,84]. During SLM, a computer-controlled system directs the laser along a predefined path derived from the 3D digital model's sliced data. The laser's energy causes the metal powder particles within the targeted zone to rapidly melt, forming a molten pool that solidifies into a metallurgically bonded state upon cooling. This layer-wise process continues, building up the final component with dense, high-integrity microstructures.

SLM overcomes many limitations of traditional manufacturing routes, especially for intricate geometries, by directly producing fully dense metal parts with superior mechanical attributes[85-88]. For instance, Wang et al. systematically examined how process parameters, such as scanning speed, laser power, and pattern spacing, influence the phase transformation behavior, mechanical robustness, and functional responses of NiTi SMAs produced via SLM[89-93]. Their studies demonstrated that the ability to customize phase transition temperatures and achieve high tensile strength makes SLM an ideal platform for engineering complex NiTi SMA architectures tailored for specific applications, such as biomedical implants or adaptive structures (see Figure 2B).

Lu et al.[94] further refined this approach by modulating laser energy input to generate NiTi microstructures featuring ultra-fine dendritic and cellular configurations. Their work achieved an unprecedented ultimate tensile strength of 776MPa, coupled with a large elastic elongation of 7.2%, and an extraordinary SME recovery rate of 98.7%. Such performance metrics open new horizons for deploying NiTi SMAs in high-performance smart systems and responsive devices (Figure 2C).

A notable innovation by Zhang et al.[56] involved implementing a stripe rotation scanning strategy to enhance the tensile and shape recovery properties of SLM-fabricated NiTi alloys. Their comprehensive microstructural analysis revealed that rapid solidification fosters the formation of a supersaturated matrix rich in vacancies and dislocations, fundamentally shaping the alloy's microstructure[95,96]. This rapid thermal cycling, characterized by frequent reheating and cooling, induces a high dislocation density and stabilizes twin structures, critical to the shape memory behavior[97,98].

Table 1 summarizing key properties such as transformation temperatures, recoverable strain, and fatigue life reported in recent studies, The table oversimplifies SME and superelasticity. Include quantitative metrics (e.g., strain recovery, hysteresis) and fabrication influences. This table highlights both the advantages and current limitations of AM processes relative to conventional methods, providing a clearer understanding of the microstructure-property relationships and guiding future research directions.

Table 2 highlights that the SME primarily relies on thermal cycling to induce martensitic transformation, with strain recovery up to 10% occurring over seconds to minutes, and exhibits a wide thermal hysteresis of 20-50°C. In contrast, superelasticity is stress-driven, enabling near-instantaneous strain recovery of up to 12% with narrow mechanical hysteresis, making it suitable for dynamic applications such as damping. Quantitative metrics like hysteresis width and recovery speed differentiate these phenomena, while fabrication methods such as LPBF influence residual stresses and phase transformation temperatures, affecting both SME and superelasticity performance. Understanding these parameters is essential for optimizing material behavior in specific applications.

AM-fabricated SMAs show shifted transformation temperatures due to rapid cooling and residual stresses, but they exhibit enhanced shape recovery and superelastic strains thanks to refined microstructures. While their fatigue life improves with post-treatment, it still lags behind conventional wrought alloys. The rapid solidification in AM results in finer grains and near-full density, although surface roughness and residual stresses require post-processing. Overall, AM offers advantages in complex geometry fabrication, though some properties like corrosion resistance are comparable or slightly affected (Table 3).

The precision of SLM fundamentally depends on the accurate regulation of parameters like laser power and scan speed. Fine-tuning these variables ensures optimal melting, minimizes residual stresses, and prevents defects such as porosity or warping. For biomedical applications, this degree of control yields highly customized implants and tissue scaffolds with complex geometries and predictable functional responses, laying the groundwork for personalized medicine and regenerative therapies (Figure 6)[99,100].

4.1.2 Copper-based SMAs (Cu-based SMAs)

Replacing NiTi with Cu-based SMAs for advanced applications necessitates overcoming specific challenges related to their intrinsic microstructural and thermomechanical properties. Cu-based SMAs, such as Cu-Al-Ni[101-105], Cu-Zn-Al[106-111], Cu-Al-Be[112-117], and Cu-Al-Mn[118-122] exhibit promising functional characteristics including high transformation strains, rapid response, and cost-effectiveness; however, their susceptibility to grain coarsening, phase instability, and brittleness complicates their fabrication and application[123].

SLM can employ a highly focused, high-energy laser beam to selectively fuse Cu-based SMAs layer by layer, enabling the realization of geometries that are otherwise difficult or impossible to produce via traditional subtractive methods[124,125]. The printing parameters of SLM must be optimized to ensure complete fusion, minimize porosity, and promote desirable microstructural features that influence the functional properties of the final component[126].

The rapid thermal cycles inherent to SLM, characterized by high cooling rates often exceeding 10^6K/s, can induce significant residual stresses, microstructural heterogeneities, and phase transformations within Cu-based SMAs[127-131]. Such rapid solidification can lead to grain refinement, but may also cause undesirable phase segregation or the formation of non-equilibrium phases, which can

Table 1. Comparative Analysis of SMA Fabrication Methods - Traditional vs. AM (LPBF/EBM)

Property	AM-Fabricated (LPBF)	AM-Fabricated (EBM)	Conventional (Cast/Wrought)	Key Insights	References
Transformation temp. (°C)	NiTi: A_f=50-110 (tunable)	NiTi: A_f=30-120	NiTi: A_f=20-110	LPBF/EBM enable wider tuning via parameters; EBM closer to conventional ranges.	[24,30,56,84,92]
Recoverable strain (%)	NiTi: 6-8%	NiTi: 4-8%	NiTi: 6-10%	Slightly lower in AM due to porosity; LPBF matches wrought NiTi.	[32,45,55,58]
Fatigue life (cycles)	10^4-10^5 (@2% strain)	10^5-10^6 (@2% strain)	10^5-10^7 (wrought)	EBM>LPBF>cast (EBM's preheating reduces residual stresses).	[21,55,67,76]
Density (% theoretical)	98-99.9%	99.5-99.9%	~100%	LPBF achieves near-full density with optimization; EBM consistently high.	[46,75]
Residual stress (MPa)	200-800	50-300	<100 (annealed)	LPBF induces higher stresses; EBM mitigates via high-temperature build.	[58,67]
Corrosion resistance	High (low impurities)	High	High	LPBF reduces impurities vs. casting; EBM avoids oxidation.	[22,58]
Energy dissipation	Cu-Al-Ni: High hysteresis	-	Cu-Al-Ni: Moderate	AM enhances damping via refined grains (LPBF).	[9,10,64]
Geometry complexity	High (lattices, gradients)	Moderate (supports needed)	Low (limited by tooling)	LPBF excels in intricate designs; EBM constrained by powder size.	[46,55,75]
Surface finish	Moderate (post-processing needed)	Rough (higher than LPBF)	Smooth (machined)	LPBF offers better resolution; EBM requires less support but coarser finish.	[51,55,75]

Notes: (A_f) stands for the austenite finish temperature.

Table 2. The Table Oversimplifies SME and Superelasticity. Include Quantitative Metrics (e.g., strain Recovery, Hysteresis) and Fabrication Influences

Property	SME	Superelasticity	Key Difference	References
Trigger	Temperature change (heating/cooling).	Mechanical stress (no temp. change).	SME requires thermal cycling; superelasticity is stress-driven.	[1-3,6-10]
Recovery Mechanism	Heating above A_f reverts martensite→austenite.	Unloading reverts SIM→austenite.	SME is thermally activated; superelasticity is mechanically reversible.	[13,80-82]
Critical Temperatures	M_s, M_f, A_s, A_f define hysteresis.	Only A_f is critical (must be>A_f for reversibility).	SME depends on full transformation range; superelasticity requires $T>A_f$.	[4,5,80]
Strain Recovery	Up to 8-10% (NiTi), but slower (seconds to minutes).	Up to 10-12% (NiTi), near-instantaneous (milliseconds).	SME is time-dependent; superelasticity is rapid.	[6-10, 82]
Hysteresis Loop	Wide thermal hysteresis (ΔT=20-50°C).	Narrow mechanical hysteresis (stress-dependent).	SME hysteresis is thermal; superelasticity is stress-based.	[9,10,82]
Energy Dissipation	Low (primarily for actuation).	High (ideal for damping, e.g., Cu-Zn-Al).	Superelasticity excels in energy absorption.	[9,10,16]
Applications	Actuators, thermal switches, aerospace deployables.	Biomedical stents, seismic dampers, eyeglass frames.	SME for slow, temp-driven tasks; superelasticity for dynamic loads.	[11-15,66]
LPBF Fabrication Impact	Residual stresses can alter M_s/A_f.	Laser parameters affect critical stress for SIM.	LPBF tuning is distinct for each property.	[24-25,56-58]

detrimentally affect the shape memory and superelastic properties[50]. Consequently, process strategies such as preheating the powder bed, optimizing laser scan strategies to control heat flow, and implementing post-processing heat treatments are critical to achieving microstructures with balanced strength, ductility, and functional stability[132].

Microstructural control is further complicated by the alloy

Table 3. Comparison of AM-Fabricated vs. Conventional SMAs

Property	AM-Fabricated SMAs	Conventional SMAs	Remarks
Transformation temperatures (°C)	NiTi: 0-50 (Ms), Cu-based: -20-0 (Ms)[56,57]	NiTi: -30-10 (Ms)[22]	AM exhibits shifted ranges due to rapid cooling, residual stresses, and non-equilibrium microstructures.
Shape recovery strain (%)	NiTi: 6-8%, Cu-based: 10-12%[61,63]	NiTi: 4-6%, Cu-based: ≤8%[8,10]	AM's refined grains and reduced defects enhance recoverable strain.
Superelastic strain (%)	4-6% (NiTi), up to 8% with optimization[7,30]	3-5% (NiTi)[8]	LPBF enables finer martensitic variants, improving superelasticity.
Fatigue life (cycles)	10^4-10^5 (as-printed), >10^6 after post-treatment[58,67]	>10^6-10^7 (wrought)[11,21]	AM fatigue life improves with heat treatment but lags behind wrought alloys.
Residual stress (MPa)	50-200 (as-printed), <50 after annealing[12,68]	<20 (hot-rolled)[13]	LPBF's rapid cooling induces stresses; post-processing mitigates them.
Microstructure (grain size)	1-10μm (LPBF), nanoscale precipitates[26,29]	10-100μm (cast/rolled)[15,18]	AM's rapid solidification refines grains, enhancing strength.
Density (% Theoretical)	98-99.5% (LPBF)[46,50]	>99.9% (wrought)[17]	Near-full density achievable with optimized LPBF parameters.
Surface roughness (μm)	1-5 (as-printed), <1 after polishing[18,55]	0.2-0.5 (polished)[19]	AM requires post-processing for smooth surfaces.
Corrosion resistance	Comparable in inert environments; surface oxidation possible[20,22]	Slightly better in some cases[21]	AM's oxide layers may affect biocompatibility (e.g., NiTi implants).
Manufacturing time & cost	Faster for complex geometries; high initial setup cost[22,47]	Slower for complex parts; high material waste[23]	AM excels in customization and lightweight structures (e.g., lattices)

composition. For instance, in Cu-Al-Ni SMAs, controlling the size and distribution of precipitates, as well as the stability of the β-phase, is crucial for tailoring the transformation temperature and hysteresis[133]. Alloying modifications, such as adding Ti, Zr, V, or B, have been explored to enhance grain boundary strengthening, suppress undesirable phase formation, and improve thermal stability, factors that are essential for maintaining functional performance under cyclic thermomechanical loading[134].

The integration of AM with Cu-based SMAs offers significant advantages, including the ability to fabricate geometrically complex, functionally graded components with internal features designed for specific actuation or sensing functionalities. This capacity is vital for developing next-generation smart devices, microactuators, and biomedical implants that require precise control over their microstructure and functional properties[135-140]. However, realizing this potential demands an in-depth understanding of the interplay between process parameters, alloy chemistry, and microstructure evolution. Advances in real-time monitoring and in-situ analysis during SLM processes are expected to further optimize fabrication protocols and enhance the reproducibility and performance of Cu SMA components[141].

In a relevant study, Tian et al.[142] a novel Cu-13.5Al-4Ni-0.5Ti SMA was successfully fabricated by SLM, demonstrating the feasibility of AM for high-performance SMAs. By meticulously optimizing the SLM process parameters, near-full density samples were achieved, exhibiting refined microstructures and enhanced mechanical properties. Microstructural analysis revealed that the rapid cooling rates intrinsic to SLM markedly influenced the phase constitution and grain structure. Notably, only the β1′ martensitic phase was detected, attributable to the extremely short solidification time that inhibits the formation of α and γ2 phases typical in conventional casting processes. The grains exhibited significant refinement, with an average size of approximately 43μm, substantially smaller than their cast counterparts, facilitated by rapid solidification and Ti-induced grain refinement mechanisms. Additionally, the presence of nanoscale Cu_2TiAl intermetallic particles (20-50nm) was observed, which contributed to the strengthening of the material.

The mechanical evaluation indicated that the SLM-fabricated alloy possesses superior tensile performance at room temperature, with ultimate tensile strengths reaching approximately 541MPa and elongations around 7.63%. These enhancements are primarily attributed to grain refinement effects and the suppression of brittle γ2 phases, which often compromise ductility. Furthermore, tensile testing at 200°C revealed an increase in both strength and ductility, up to approximately 611MPa and 10.78% elongation, largely due to the stability of the BCC parent phase and the activation of stress-induced martensitic transformations, which enhance ductility and energy absorption. The microstructures demonstrated a distinct difference from cast alloys, with finer grains and a more uniform phase distribution, underpinning these improved properties.

The influence of process parameters, particularly laser energy density, was systematically examined, revealing

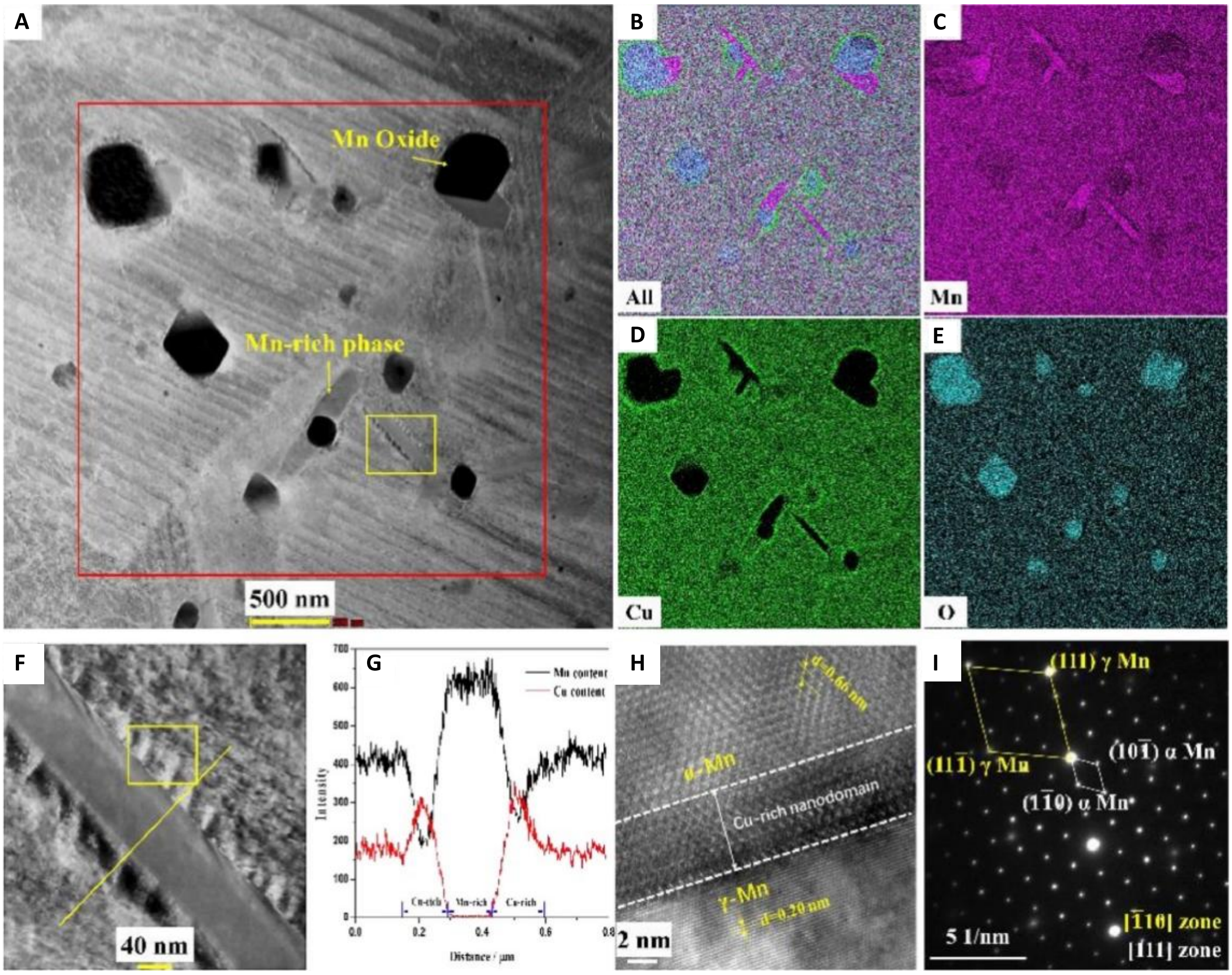

Figure 6. Bright-field Transmission Electron Microscopy (TEM) Micrograph of Mn-30 wt.% Cu Subjected to SLM Followed by Heat Treatment. (A) Elemental distribution maps for all elements (B), Mn (C), Cu (D), and O (E) within the region marked by the large red box in (A). Figure 8f provides a magnified view of the area outlined by the small yellow box in (A). The distributions of Mn and Cu along the yellow line shown in (F) are depicted in (G). High-resolution TEM image of the region indicated by the yellow box in (F) is shown in (H), with the corresponding Selected Area Electron Diffraction (SAED) pattern in (I). Reprinted with permission from Ref.[99]

that moderate energy inputs (~107J/mm³) optimize density and mechanical performance. Excessive energy led to pore formation and voids due to incomplete melting or spheroidal particle agglomeration, which adversely affected the integrity of the final component. The hardness values ranged from 267 to 289HV, correlating with microstructural refinement and intermetallic formation[142].

Tian et al.[143] demonstrated the successful use of SLM to produce high-quality Cu-based shape-memory alloys with the composition 81.95Cu-11.85Al-3.2Ni-3Mn (wt.%). Optimized processing parameters, particularly laser power, scanning speed, and strategy, enabled the fabrication of dense, nearly fully martensitic samples with up to 99% relative density. The high cooling rates inherent to SLM suppressed secondary phase formation, favoring the β′-martensite structure essential for shape-memory effects.

Microstructural analysis showed that the processing strategy significantly influences porosity, pore distribution, and grain morphology. The single-track approach allowed precise parameter adjustment, with optimal energy input around 30-40J/mm³, resulting in dense, high-quality parts. Pore characteristics and grain sizem, ranging from about 40μm in bulk to under 10μm in overlap zones, were strongly affected by the heat flow and energy input, with remelting refining grains and improving surface finish. The refined microstructure contributed to promising mechanical properties, confirming SLM's potential for tailoring microstructures and producing complex, high-density Cu-based SMAs. Further work on mechanical and shape-memory behavior will clarify the full advantages of AM over conventional methods, paving the way for advanced smart components with customized microstructures and enhanced functionalities[143].

Cu-Al-Ni SMAs are known for their high thermal stability and a range of potential uses. However, their practical application is often limited by their relatively low elastic strain and subpar shape memory performance, specifically their recoverable strain. Additionally, introducing new reinforcing elements typically leads to a polycrystalline structure with larger grain sizes, which is not ideal for maintaining shape memory properties. To address these issues, Abolhasani et al.[144] study proposes a novel approach to enhance both the SME and its stability in Cu-Al-Ni SMAs by partially reinforcing the material with alumina (Al_2O_3) using SLM. In this method, the reinforcement lines are deposited in-plane at the mid-height of the printed component, positioned in the neutral plane. The impact of partial reinforcement is evaluated by comparing samples with 0.3wt% and 0.9wt% Al_2O_3 to fully reinforced counterparts. Findings reveal that the localized residual compressive stresses generated in the neutral plane during SLM, particularly above the reinforcing lines, contribute to an improved SME. This improvement is attributed to increased mechanical anisotropy along the build direction. Furthermore, a novel phenomenon termed the "waistband effect" is observed during cyclic compression tests, where the reinforcing particles gradually penetrate deeper into the neutral plane with each cycle. This process enhances strain recovery, especially in partially reinforced samples. Overall, these results demonstrate that partial reinforcement with Al_2O_3 significantly boosts the shape memory performance of Cu-Al-Ni SMAs[144].

In another study, Gustmann et al.[145] applied an additional remelting step during the fabrication of an 81.95Cu-11.85Al-3.2Ni-3Mn SMA via SLM. Using a single-track technique followed by bulk remelting, the process parameters were optimized to control remelting depth and influence material properties. While no clear correlation between energy input and relative density was found, optimal results (~99.5±0.3%) were achieved at around 36 J/mm³, comparable to SLM bulk samples with 98.9±0.1%. X-ray tomography showed that increasing density mainly involved eliminating pores smaller than 100μm. Grain size remained mostly unaffected at lower energies but coarsened significantly between 100 and 250J/mm³. Transformation temperatures could also be tuned via process parameters, with peak martensitic transformation temperatures adjustable between 90°C and 120°C through remelting. The samples exhibited excellent deformability under compression and tension. Despite changes in pore and grain sizes, their mechanical properties stayed stable. Overall, the additional remelting step enables the production of dense, fully martensitic components with controlled transformation temperatures, without compromising mechanical performance (Figure 7)[145].

Dennis et al.[146] aimed to compare and analyze the microstructural characteristics and thermal stability of a Cu-11.3Al-3.2Ni-3.0Mn-0.5Zr SMA produced by two different methods: SLM and traditional powder metallurgy (PM). The PM samples were created by sintering pre-alloyed powders (106-180μm) in an argon atmosphere at 1060°C, without any additional processing. In contrast, SLM specimens were formed by melting pre-alloyed powders (32-106μm) onto a Cu-10Sn substrate. Both processing routes resulted in the formation of β′1 martensite; however, the PM samples exhibited coarser martensitic variants. Additionally, the PM specimens contained intergranular eutectoid phases and stabilized austenite at room temperature. Hardness measurements showed similar average values for both sets, though the standard deviation was higher in SLM samples due to porosity. The SLM-processed specimens displayed reversible martensitic transformations with a T_0 of 171°C, whereas the PM samples did not exhibit SMEs[146].

Shishkovsky et al.[147] examined the synthesis of intermetallic phases during layer-by-layer SLS/melting of Cu-Al-Ni powders. Using optical and scanning electron microscopy, energy-dispersive X-ray spectroscopy (EDX), and X-ray diffraction (XRD) analysis, the microstructure and intermetallic phases in porous 3D samples were characterized under various laser processing conditions. The prepared mixtures demonstrated high laser sintering ability, and the SME was confirmed through specific electrical resistance measurements. Porosity in the laser-synthesized Al_7Cu_4Ni intermetallic caused a shift in the temperature peaks, with the austenite transformation interval (As-Af) ranging from 50 to 80°C, and the martensite transformation (Ms-Mf) from +25 to -40°C.

In the first application of two-zone SLM to produce CuAlNi intermetallics, samples were fabricated with an 80μm hatch distance, 70W laser power, 70μm beam diameter, and scan velocity of 140mm/s. The process, conducted in argon, tended to produce heterogeneous rhombohedral Al_7Cu_4Ni phases, with scanning electron microscope (SEM) and EDX revealing uncontrolled Al oxidation. Electrical resistance evolution during synthesis confirmed the presence of phases and SME behavior in porous Cu-Al-Ni samples. The electrical resistance measurement proved effective for identifying phase transformations and estimating the temperature range of SME. Porosity caused the transformation peaks to shift, with the As-Af interval between 50-80°C and Ms-Mf between +25 and -40°C.

This approach enables the use of electrical resistance as a feedback tool for actuator control without additional sensors. The layer-by-layer SLS/SLM fabrication of porous Cu-Al-Ni offers potential for advanced bio-MEMS devices, sensors, implants, and orthopedic applications, including self-initiating and self-fixing prosthetic elements that operate at human body temperature[147].

Pérez-Cerrato et al.[148] demonstrates a complete SLM process for Cu-Al-Ni SMAs, optimizing parameters to

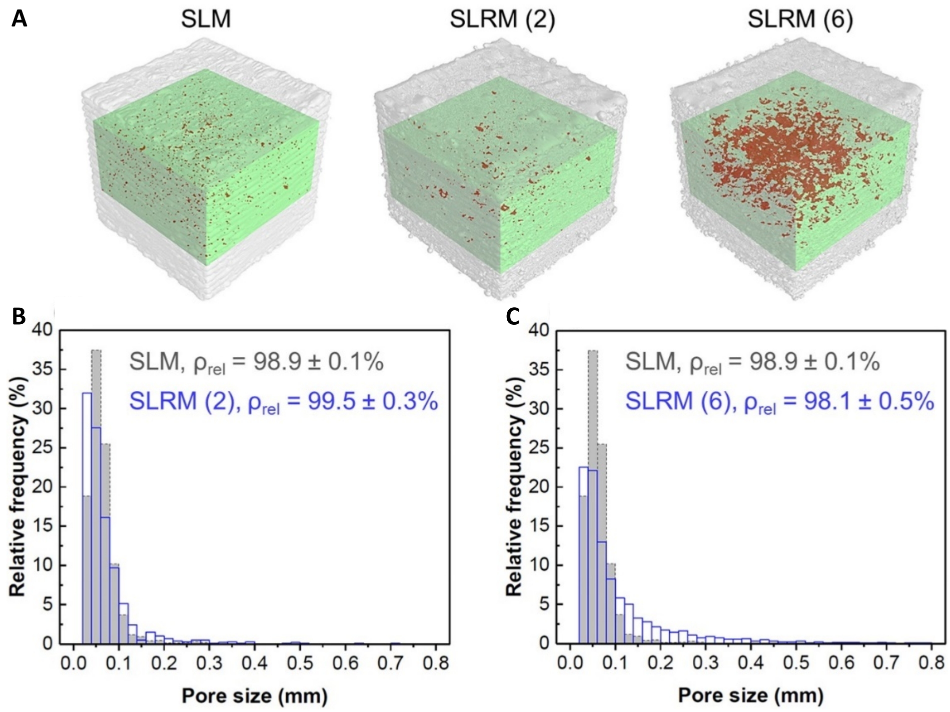

Figure 7. The μ-CT Reconstruction and Pore Size Distribution of Additively Manufactured Cu-Al-Ni-Mn Cubes via Different SLM and SLRM Techniques. μ-CT reconstruction of additively manufactured cubes composed of 81.95Cu-11.85Al-3.2Ni-3Mn, shown in (A). The images correspond to specimens produced via SLM, SLRM (2), and SLRM (6) techniques (refer to Table 2). The analyzed volume, measuring 7×7×5mm³, depicts the material in green and pores in red. The pore size distributions for the remelted samples, compared to the original SLM sample, are presented in (B) and (C). Remelting under specific parameters (SLRM (2)) effectively reduces smaller pores. However, excessive remelting energy can lead to increased overall porosity, with larger pores also becoming evident. Reprinted with permission from Ref.[145]

achieve high compaction and functional performance. Microstructural analysis showed columnar grains with a texture along the build direction, enhancing superelasticity and shape memory. Fully recoverable superelastic strain of 2.7% and shape memory recovery of ±4% bending strain were obtained, outperforming reference PM samples.

A comprehensive process route included atomization, SLM fabrication with powders of 15-45μm, and post-treatments like hot isostatic pressing (HIP) and thermal aging. Optimal energy density (~117J/mm³ at 350W) ensures complete melting, while HIP reduces porosity and stabilizes microstructure. Thermal treatments restore microstructure and transformation temperatures, ensuring reliable SME. The columnar microstructure with texture improves functional behavior in the build direction, with stable superelastic cycles and full shape memory recovery[148].

Pérez-Cerrato et al.[149] revealed the potential of SLM for producing Cu-Al-Mn SMAs with enhanced superelasticity. An additional remelting step during LPBF was systematically investigated by varying hatching distance and scanning speed to optimize density and transformation temperatures. Results showed that remelting improves microstructure and superelastic properties, enabling the fabrication of locally tailored SMA components for application-specific scenarios.

Furthermore, a comprehensive processing route for Cu82.2Al13.3Ni4.5 (wt.%) SMA was developed, involving atomized powders, LPBF fabrication with optimized parameters (e.g., energy density of 117J/mm³ and 350W laser power), and post-processing treatments like HIP and thermal aging. Microstructural analysis revealed a columnar grain structure with a texture aligned with the build direction, which enhances functional behavior. Superelastic strains up to 2.7% and full shape memory recovery after ±4% bending strain were achieved, with the microstructure and properties preserved through post-processing. Overall, SLM significantly improves the functional performance of Cu-Al-Ni SMAs, approaching the levels seen in PM-produced counterparts. Controlling process parameters and texture during building can further enhance these properties, paving the way for advanced AM applications in shape memory and superelastic devices[149].

Zhuo et al.[150] represents the first investigation into fabricating CuZnAl SMAs via SLM, focusing on how process parameters influence microstructure and material properties. The results reveal that energy density plays a crucial role in determining the final characteristics of the fabricated samples, primarily through its effect on zinc evaporation. As the energy density increases, the relative density of the samples initially improves, reaching over 99.9% at an optimal value of 277.8J/mm³. However, excessive energy input causes significant Zn evaporation, leading to porosity and a decline in density. The phase constitution of the alloys also varies with energy density: lower energy levels retain more Zn, resulting in a microstructure dominated by brittle β′ martensite with needle-like morphology, while higher energy densities diminish Zn content and favor the formation of the α phase with rod-like or equiaxed structures. This transition impacts mechanical and thermal behaviors, as evidenced by DSC analysis, where the intensity of martensitic transformation peaks decreases with increasing energy density, reflecting a reduction in reversible martensite due to phase stabilization effects from Zn loss. Microhardness measurements showed a decline from 236.8HV to 167.6HV as energy density rises, but fracture strength and irrecoverable strain improve, owing to increased α phase content and decreased porosity. Overall, these findings demonstrate that by carefully adjusting laser energy input, it is possible to tailor the phase composition, microstructure, and mechanical properties of SLM-fabricated CuZnAl alloys, paving the way for producing high-performance shape memory components with customized characteristics[150].

Harnessing the power of SLM, researchers have crafted a cutting-edge Cu-11.85Al-3.2Mn-0.1Ti SMA that defies convention[151]. By fine-tuning energy density, the alloy's grains were shattered into ultrafine structures, shrinking to an average width of just 0.15 micrometers, resulting in a remarkable 90% refinement over traditional cast counterparts. This nano-sized revolution triggers a dual-strengthening mechanism: densely packed Cu_2TiAl precipitates interweave with dislocations, forging a formidable network that boosts mechanical resilience. The outcome showed an impressive room-temperature tensile strength of 829MPa with a modest 6.4% fracture strain, and an even more formidable 883MPa coupled with 12% strain at 200°C, nearly 30% stronger than existing laser-melted quaternary Cu-based SMAs. Microstructurally, the SLM process crafts an intricate mosaic, equiaxed crystals aligned along the scan path and elongated formations along the build direction, leading to a slight but significant anisotropy in hardness. These tailored microstructures underpin the alloy's superior superelasticity and shape memory capabilities[151].

Xi et al.[152] demonstrated the successful fabrication of a cost-effective Cu-11.85Al-3.88Mn-1.6Nb SMA using SLM, showcasing remarkable functional properties. By adjusting laser energy inputs between 123 and 185J/mm^3, researchers achieved microstructures featuring a mix of 18R and 2H martensite, along with nanoscale $(Cu, Mn)_3Al_3Nd_4$ precipitates that enhance strength and stability. The powder itself exhibited excellent fluidity and uniformity, facilitating consistent melting.

As laser energy increased, the dominant martensitic phase shifted toward 2H, and transformation temperatures gradually rose due to Mn evaporation. Despite microstructural inhomogeneities at higher energies, the alloy delivered impressive mechanical performance with a compressive strength of 1652MPa and 15.1% strain, alongside an outstanding shape memory recovery of over 99%. Nano-sized precipitates approximately 100nm in size were observed (Figure 5). EDS analysis revealed atomic percentages of Cu, Al, Mn, and Nd as 24.68%, 30.49%, 4.72%, and 40.09%, respectively. The atomic ratio of (Cu, Mn): Al: Nd was close to 3:3:4, indicating that the second phase can be considered $(Cu, Mn)_3Al_3Nd_4$. These precipitates have a semi-coherent relationship with the matrix, which contributes to the high strength and excellent mechanical properties of the alloy[152].

Babacan et al.[153] showcased how LPBF can produce dense, crack-free Cu71.6Al17Mn11.4 SMA specimens with highly tailored microstructures. By adjusting process parameters, particularly energy input, the grain size and transformation temperatures could be precisely controlled, higher energy inputs shifted transformation temperatures upward. Notably, the rapid cooling during AM prevented the formation of α-phase precipitates that hinder martensitic transformation, eliminating the need for post-process heat treatments used with cast materials. The additively manufactured samples displayed fully austenitic structures with fine columnar grains aligned along the building direction (BD), resulting in enhanced yield strength and superelasticity compared to traditional cast alloys. A maximum recoverable strain of 2.86% was achieved after compressive loading, highlighting the technique’s potential for producing custom-designed, superelastic Cu-Al-Mn parts. These findings suggest that LPBF is a promising route for creating high-performance, room-temperature superelastic components with microstructure-driven properties, paving the way for tailored, application-specific shape memory devices (Figure 8)[153].

Wu et al.[154] demonstrates that SLM can produce highly oriented, columnar Cu71Al18Mn11 SMAs with exceptional superelasticity. Using an orthogonal design, optimal parameters, such as 240W laser power, 1,000mm/s scanning speed, 0.11mm scanning distance, and 25μm layer thickness, were identified to achieve nearly full density (99.18%) and a strong texture. The resulting microstructure, predominantly β-phase, exhibited superior compression strength and notable superelastic strains, especially along the scanning direction with 2.50%, surpassing the 2.32% along the BD. The study highlights how the interaction of process variables influences melt pool size and microstructure orientation, offering a promising route to tailor Cu-Al-Mn SMAs with enhanced superelastic properties and complex geometries. Overall, SLM presents a straightforward method for fabricating textured, high-performance shape memory parts for advanced applications[154].

Niedbalski et al.[155] investigated laser-assisted synthesis as a promising approach for fabricating dense Cu-Al-Ni

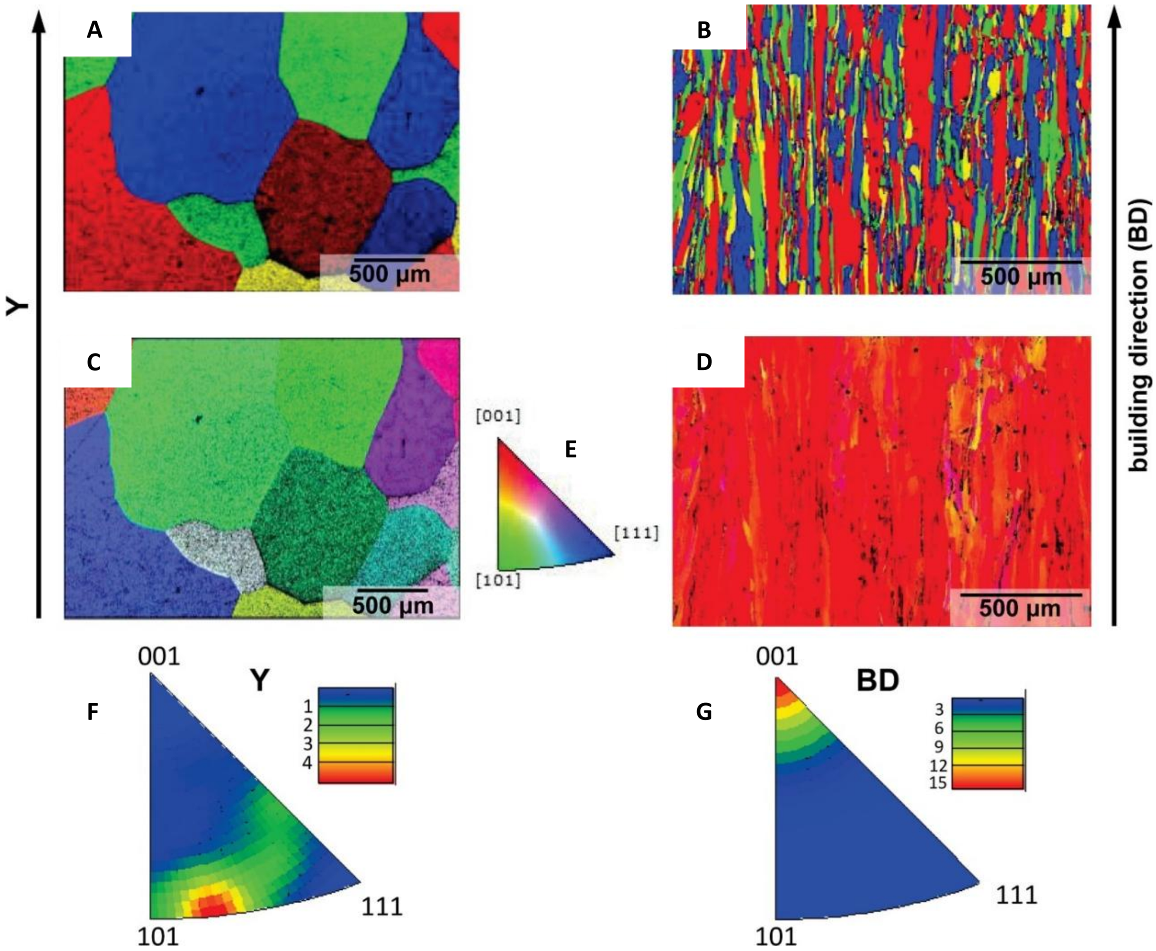

Figure 8. Microstructural Characterization by EBSD of Cast Heat-treated and SLM-Ref Samples. Electron backscatter diffraction (EBSD) maps illustrating the microstructure along the Y direction of the cast heat-treated (HT) samples in (a, c, f), and along the BD of the SLM-Ref specimens in (b, d, g). The detailed overview includes (a, b) grain maps of the austenite phase, (c, d) grains color-coded according to their texture (also shown in (e)), and (f, g) inverse pole figures . The central image (e) displays the IPF coloring scheme used for the maps in (c) and (d). Reprinted with permission from Ref.[153]

SMAs with potential for large-scale AM. By laser melting elemental powders in a controlled argon atmosphere, alloys with 14.2% Al and Ni content between 2-4% were produced, exhibiting martensitic microstructures capable of phase transformations between 85°C and 192°C. The research revealed that increasing inert gas pressure suppresses the austenite-to-martensite transformation, leading to reduced microhardness and transformation enthalpies, likely due to hindered volumetric transformation. Conversely, lower gas pressures increased residual oxygen, causing oxidation and affecting alloy quality. Shorter solidification times at higher pressures resulted in purer, lower-hardness alloys. While the transformation temperatures were indirectly influenced via microstructure, the transformation enthalpy was directly affected by gas pressure, correlating with the hindrance of phase transformation. Porosity mainly stemmed from gas release rather than incomplete melting or voids. Overall, the findings demonstrate that laser-assisted synthesis can efficiently produce high-density Cu-Al-Ni SMAs, but further understanding of the microstructural evolution under varying processing conditions is essential to advance this technique toward AM of complex, high-performance SMA components[155].

Singh et al.[126] demonstrated the successful fabrication of dense Cu-Al-Ni-Mn SMA structures via SLM using ball-milled elemental powders. By optimizing laser power between 300-400W, the study achieved samples with up to 99% density, minimal porosity, and excellent mechanical properties, hardness reaching 380HV and tensile strength of 1550MPa. Lower laser powers caused incomplete fusion and porosity, while higher powers increased grain size and thermal shrinkage. All samples exhibited the β martensite phase, with the most optimal at 350W, producing defect-free, well-bonded microstructures with refined grains. The transformation temperature and sharpness improved with increased laser power, indicating enhanced phase transformation behavior. The findings open pathways for cost-effective, powder-based AM of dense SMA components, with future prospects including HIP and post-heat treatments to further enhance microstructure and shape recovery capabilities[126].

Singh et al.[156] explored how HIP temperature influences the density, microstructure, and mechanical properties of Cu-Al-Ni-Mn SMAs produced by SLM. HIP treatment increased density by 11.5%, with optimal pore shapes, spherical and small, observed at 950°C, while higher temperatures introduced non-spherical pores. SEM imaging showed the elimination of shrinkage porosity and grain growth with rising HIP temperatures. XRD analysis revealed phase transformations and changes in crystallite size, correlating with improved microhardness and tensile strength, especially at 950°C. These findings demonstrate that controlled HIP processing enhances the mechanical performance of SLM-fabricated Cu-Al-Ni-Mn alloys, with temperature optimization being key to balancing density and microstructural refinement, paving the way for advanced industrial applications[156].

Felice et al.[157] investigated the successful production of Cu-17Al-11.4Mn (atomic %) SMA components through arc-based AM utilizing a gas metal arc welding (GMAW) system. The deposition resulted in a defect-free wall with a uniform microstructure. Analysis using optical microscopy, electron microscopy, and synchrotron X-ray diffraction confirmed the development of a columnar grain structure, attributed to thermal cycling effects, and predominantly exhibited a FCC phase. Tensile testing in both horizontal and vertical orientations demonstrated high strength and ductility with negligible anisotropy. Additionally, superelastic cyclic tests showed consistent hysteresis behavior over 100 loading-unloading cycles, indicating excellent functional fatigue resistance. In situ synchrotron X-ray diffraction during tensile loading revealed a stress-induced phase transformation, highlighting the material's potential for superelastic applications. These findings illustrate the viability and benefits of arc-based AM for processing Cu-based SMAs, paving the way for cost-effective fabrication of functional components[157].

High-entropy alloys (HEAs) have been identified as beneficial components in SMA coatings, primarily due to their ability to refine the microstructure and consequently improve tribological properties. Casati et al.[158] investigated the $Fe_{45}Mn_{35}Co_{10}Cr_{10}$ HEA was integrated into a $Cu_{11.85}Al_{3.2}Mn_{0.1}$ SMA coating through the process of laser cladding. The study focused on examining how varying amounts of HEA influence the structural evolution, phase transformations, and wear resistance of the resulting coatings. The findings reveal that incorporating $Fe_{45}Mn_{35}Co_{10}Cr_{10}$ HEA into the SMA matrix significantly refines the microstructure, facilitating the formation of complex intermetallic compounds. This microstructural enhancement leads to a marked improvement in tribological behavior, primarily by increasing the hardness and wear resistance of the coating. The research provides valuable insights into the design of advanced, high-performance coatings for engineering applications, demonstrating that the strategic addition of HEAs can serve as an effective approach to bolster wear resistance and extend the functional lifespan of surface coatings in demanding environments[158].

Although significant progress has been made in the AM of metamaterials, there are still inherent compromises between functionality and mechanical performance due to their static structures. This limitation reduces their suitability for applications that demand high levels of multifunctionality. Zheng et al.[159] introduced an innovative method to producing multifunctional SMA metal metamaterials utilizing LPBF technology. This technique facilitates reversible superelastic strains exceeding 20%, with a complete (100%) recovery rate, an order of magnitude greater than that observed in traditional printed alloys. Such performance is achieved through a novel metamaterial structural design combined with a specially developed SMA powder. To realize these goals, the unit cells of the metamaterial were initially designed to allow flexible deformation, with a Poisson's ratio close to zero. They then synthesized a new SMA alloy composition based on Cu-18 at% Al-10 at% Mn-0.3 at% Si, which demonstrated excellent printability and compatibility with the LPBF process. The resulting printed SMA exhibited superelastic behavior, as well as one-way and two-way SMEs under different processing conditions. Moreover, by adjusting the manufacturing parameters, we successfully integrated multifunctionality into the flexible Cu-Al-Mn-based metamaterials. The fabricated metamaterial showed outstanding deformability and was capable of recovering its original shape after deformation, thanks to its superelasticity and shape memory properties. This work highlights the immense potential of AM for creating functional, adaptable metal metamaterials and introduces a new approach for developing intelligent metal-based structures.

Pérez-Cerrato et al.[160] thoroughly investigates the entire AM process chain for Cu-13.5Al-4.0Ni (wt.%) SMAs, starting from powder production via gas atomization and ending with component fabrication through LPBF. The alloy was specifically designed to exhibit martensitic transformation above room temperature, enabling the assessment of the SME through thermal activation. Throughout the research, the microstructure and transformation behavior were examined at various stages, including the initial atomized powder, LPBF-processed samples with single and double melting cycles, and post-processing heat treatments such as HIP.

The findings highlight that high-quality powders produced through precise gas atomization are essential, especially to control aluminum content, which significantly influences the martensitic transformation. HIP was shown to be an effective post-processing step for achieving full densification, crucial for functional applications. Thermal treatments after LPBF, or after LPBF combined with HIP, are necessary to restore and optimize the microstructure, preventing the formation of stable phases that could impair shape memory behavior.

When subjected to appropriate thermal treatments, the Cu-Al-Ni SMAs demonstrated excellent thermoelastic martensitic transformation with low thermal hysteresis (~16°C) and showed highly reproducible superelastic cycles up to 1.5% strain. The SME was successfully activated through heating in thermally treated samples, indicating promising potential for practical applications[160].

In conclusion, the synergy between Cu-based SMAs and laser-based AM techniques like SLM presents a promising pathway toward fabricating complex, high-performance smart objects for 3D/4D printing applications. Continued research focused on process optimization, alloy development, and microstructural tailoring will be essential to unlock the full potential of these materials in innovative smart device architectures.

4.1.3 Fe-based SMAs

Research specifically addressing the AM of Fe-SMA materials remains relatively scarce, despite the widespread use of AM techniques in metallic alloys, especially Ni-Ti-based systems. Among the existing studies on AM-fabricated Fe-SMAs, techniques such as LPBF and DED[161,162] are commonly preferred over SLM[163]. This preference stems from issues like pronounced surface cracking and reduced manufacturing efficiency associated with SLM when used for Fe-SMA fabrication. The upcoming sections offer a concise overview of LPBF and DED technologies, both of which have been employed for producing Fe-SMAs. These methods represent two major categories within metal AM. Although they share some similarities, they differ significantly in aspects such as material supply mechanisms and energy sources, for example, DED typically uses a laser or electron beam, while wire arc AM mainly relies on an electric arc as its energy source.

Niendorf et al.[163] demonstrated, for the first time, that an Fe-based, high Mn-Al shape memory alloy exhibiting good pseudo-elasticity can be processed by AM. The microstructural evolution during processing is strongly influenced by thermal gradients and solidification velocity, which depend on processing parameters and specimen geometry. A single-step solutionizing heat treatment induces significant grain growth, leading to microstructures that display good reversibility. Mechanical testing revealed a maximum reversible pseudo-elastic strain of approximately 7.5%. These findings highlight that microstructural design, such as establishing a coarse-grained microstructure, is essential for achieving desirable pseudo-elastic behavior. The reversibility of the martensitic transformation was confirmed through mechanical data. However, issues such as degradation during testing and surface cracking are detrimental and require further investigation. Future research should focus on microstructural engineering, such as epitaxial growth of columnar grains, to optimize properties for additively manufactured Fe-Mn-Al-Ni SMAs.

Yang et al.[164] conducted a comprehensive investigation into the orthopedic potential of biodegradable Fe-Mn-Cu alloys. Their study focused on understanding the mechanical properties, wear resistance, MRI compatibility, biodegradation behavior, antibacterial efficacy, cytocompatibility, and osteogenic differentiation capacity of these materials. They systematically characterized the microstructure, mechanical performance, and biological responses of an Fe-30Mn-6Cu alloy produced via SLM. For comparison, a Cu-free Fe-30Mn alloy was also fabricated under similar conditions. The addition of 6 wt.% Cu stabilized the γ-austenite phase, resulting in increased yield strength, enhanced wear resistance, faster electrochemical biodegradation, and strong antibacterial activity. Specifically, the SLMed Fe-30Mn-6Cu exhibited a fully γ-austenite microstructure with fine grains (~7μm) and Cu-enriched intergranular second-phase particles. It achieved a yield strength of approximately 230MPa—about 24% higher than the Cu-free alloy—and demonstrated improved tribological performance, low magnetic saturation, and susceptibility. The biodegradation rate was three times higher than the Cu-free sample, and the alloy showed over 99% bacteriostatic rate against *E. coli* and *S. aureus*. Additionally, it exhibited excellent cytocompatibility and promoted osteogenic differentiation in MC3T3-E1 cells. These findings enhance understanding of the structure-property-function relationships in multifunctional Fe-Mn-Cu alloys and highlight their potential for orthopedic implant applications.

4.3 LPBF and SLS Printing in SMA Manufacturing

LPBF shares core principles with SLM but emphasizes a layer-by-layer deposition of powdered metal, selectively melted by a focused laser beam guided by advanced galvanometric scanners. As depicted in Figure 3A, a thin layer of metal powder is evenly spread over the build platform; the laser then selectively fuses the powder in regions defined by the 3D model, repeating this cycle to produce intricate parts with high geometric fidelity and excellent surface finishes. The high energy density inherent to LPBF facilitates the rapid melting and solidification of NiTi powders, creating dense structures with complex internal geometries. Nonetheless, the process involves a delicate balance: excessive energy can induce vaporization and thermal stresses, leading to defects such as porosity or cracking. Conversely, insufficient energy results in incomplete fusion, compromising mechanical integrity (Figure 9). Recent advances have targeted micro-scale LPBF (μ-LPBF), where reducing the laser spot size, powder particle dimensions, and layer thickness allows for feature sizes below 300μm, vital for microdevice fabrication[165-172].

Xiong et al.[166] demonstrated that optimizing laser

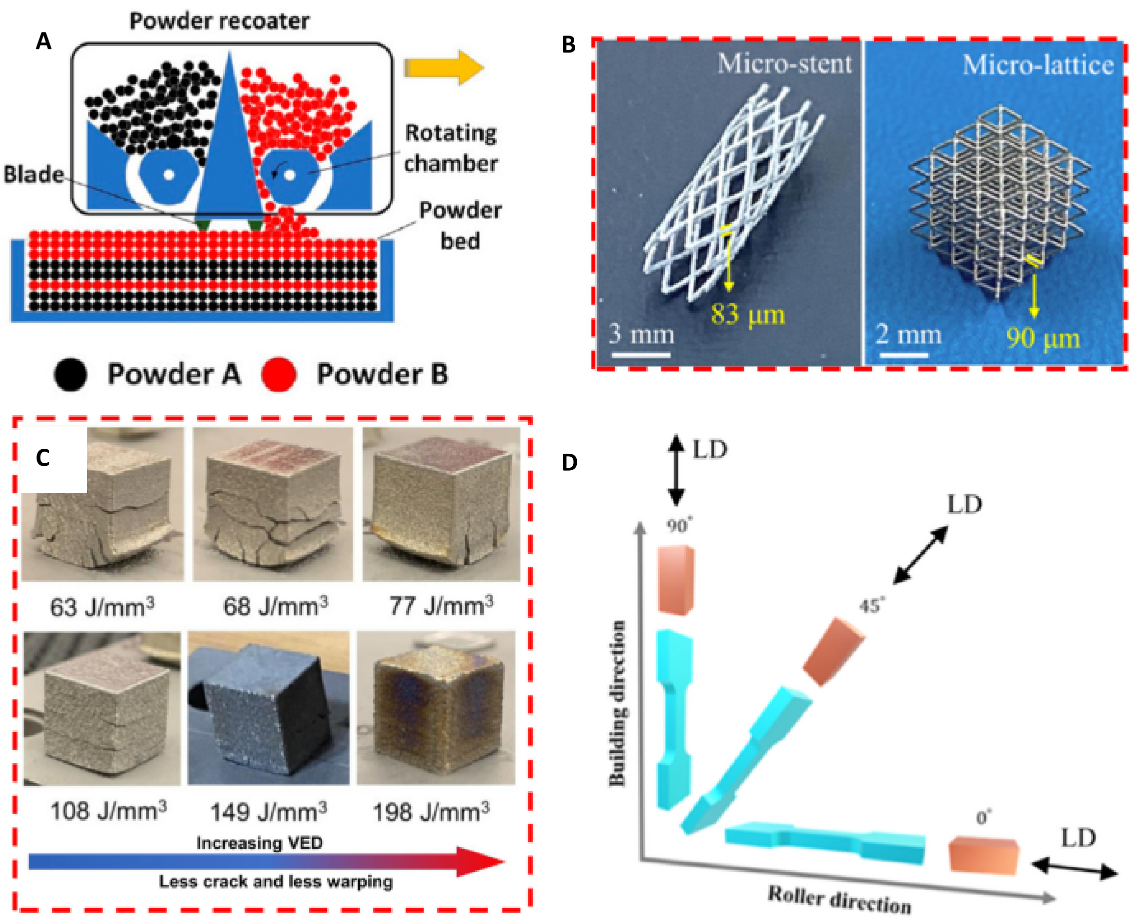

Figure 9. Overview of LPBF Process, Complex NiTi Structures, Defect Reduction with Energy Density, and Build Orientations for Structural Analysis. (A) The working principle of LPBF is illustrated in Ref.[165]. (B) Various complex structures fabricated using NiTi alloy are depicted in Ref.[166]. (C) The as-printed cubic $Ni_{51.2}Ti_{48.8}$ samples demonstrate a reduction in macroscopic defects such as cracks, warping, and delamination as the volumetric energy density increases, as shown in Ref.[167]. (D) A schematic diagram presents the arrangement of builds for structural analysis, fabricated at orientations of 0°, 45°, and 90°, under identical process parameters, as detailed in Ref.[168].

parameters with smaller laser spots and powders produced NiTi microdevices exhibiting superior shape memory and mechanical properties, distinct from those obtained via traditional LPBF (see Figure 3B). These microstructures often display fewer pores and cracks, enhancing superelasticity and functional stability, although post-fabrication heat treatments are typically needed to activate full shape memory responses.

Moreover, by adjusting parameters such as laser power and scan rate, researchers like Xue et al.[167] have suppressed defect formation, thereby significantly enhancing the superelastic behavior of printed NiTi components. Such precise control enables the fabrication of complex, load-bearing structures suitable for biomedical and aerospace applications. Additionally, Nematollahi et al.[168] explored the influence of build orientation (0°, 45°, 90° relative to the build plate) on microstructure and shape memory properties, revealing the potential to engineer anisotropic SMA components through orientation control (see Figure 3D). The continuous refinement of LPBF techniques, especially in the micro-scale domain, promises to revolutionize the production of customized biomedical devices, smart implants, and tissue scaffolds with intricate internal architectures, pushing the frontiers of personalized healthcare.

Shishkovsky et al.[173] explored the temperature-dependent electrical resistivity of porous NiTi articles fabricated through SLS, highlighting their potential for exhibiting the SME. Their investigations reveal that porous NiTi samples derived from elemental Ni and Ti powders demonstrate the likelihood of shape memory behavior within a temperature range from -50°C to 0°C. In contrast, samples produced from commercial PV N55T45 grade NiTi powder via laser sintering display this effect in a higher temperature window of +25°C to +50°C. These findings suggest that layered synthesis using SLS can produce porous NiTi structures capable of self-actuation at biologically relevant temperatures.

The presence of the SME in these porous, layer-by-layer fabricated monolayers opens promising avenues for advanced biomedical applications. Such materials could serve as self-activating implants, sensors, or devices that automatically adjust, fix, or deploy within the human body. The inherent porosity also offers a significant advantage for tissue integration, promoting soft tissue ingrowth, which enhances biocompatibility and expedites healing processes. Overall, harnessing the shape memory properties of

https://doi.org/10.53964/id.2026010

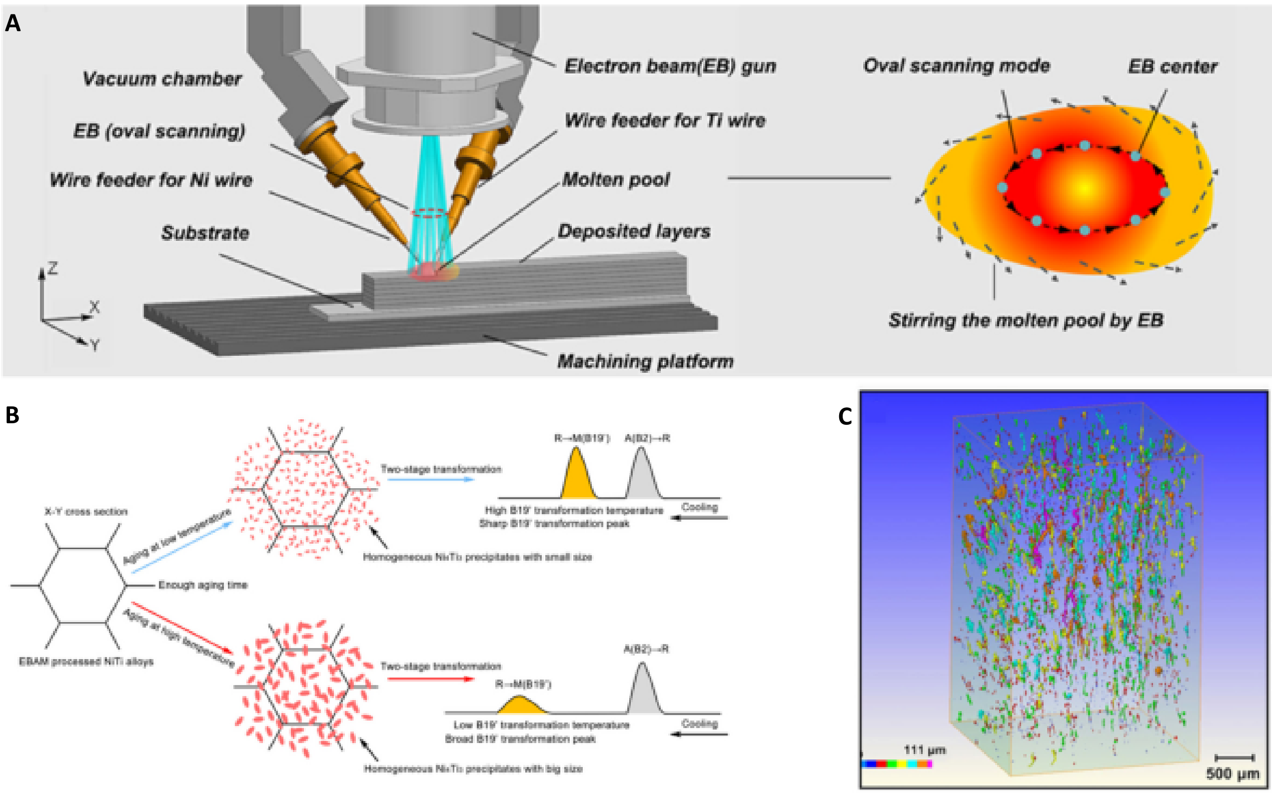

Figure 10. Schematic and Microstructural Analysis of EBM Process. (A) Schematic illustration of the EBM process. Reprinted with permission from Ref.[175]. (B) An imprinted cubic $Ni_{51.2}Ti_{48.8}$ component demonstrating that higher bulk energy density results in a reduction of large-scale defects such as cracks, warping, and delamination. Reprinted with permission from Ref.[176]. (C) X-ray computed tomography (XRT) 3D reconstructed image of an EBM-fabricated NiTi alloy. Reprinted with permission from Ref.[177].

SLS-produced porous NiTi paves the way for innovative solutions in orthopedics and regenerative medicine, elevating the functionality and effectiveness of future implantable devices[173].

Xue et al.[174] reported that porous titanium and nitinol implants can be precisely fabricated via SLS/Melting, offering superior control over composition, porosity, and near-net-shape production. The process's rapid cycle and high temperatures minimize contamination and energy use, producing high-quality, biocompatible structures. Notably, porous NiTi exhibits a martensitic transformation around -50°C to 0°C, indicating shape memory capabilities suitable for biomedical applications. Histological analysis shows excellent biocompatibility, with no corrosion or adverse tissue reactions, and strong bone integration akin to native tissue. Cell culture studies demonstrate that these porous implants support cell adhesion, proliferation, and differentiation, especially when combined with hydroxyapatite. Overall, SLS-produced porous Ti and NiTi show immense promise for advanced tissue engineering, craniofacial, and load-bearing implants, combining mechanical performance with biological compatibility[174].

4.2 EBM for SMAs Fabrication

4.2.1 NiTi-based Objects

EBM, pioneered at the University of Gothenburg and later commercialized by Arcam (acquired by GE Additive in 2016), represents a distinctive subset of powder bed fusion technologies that utilize a high-energy electron beam as the heat source. Unlike laser-based methods, EBM operates within a vacuum chamber, which prevents beam scattering and reduces contamination, thereby enabling the production of high-purity, dense metallic components[175-177].

Fundamentally, EBM employs an electron gun that accelerates electrons to generate a focused, high-intensity beam directed at a powder bed. The process begins with preheating the entire build chamber to elevated temperatures, up to 1000°C, facilitated by the electron beam itself. This preheating reduces residual stresses, minimizes thermal gradients, and promotes uniform melting. As depicted in Figure 4A, the electron beam selectively scans the powder layer in accordance with the sliced 3D data, fusing particles into a cohesive solid during each pass (Figure 10).

A key advantage of EBM is its capacity for rapid layer deposition at elevated temperatures, which facilitates the formation of microstructures with reduced residual stresses and improved mechanical properties. The process's high thermal input allows for the direct fabrication of complex, dense NiTi SMA structures with minimal post-processing. In addition, the absence of support structures, thanks to the self-supporting nature of the partially melted powder, reduces material usage and simplifies removal[178-184].

Research by Pu et al.[176] demonstrated that tailored heat treatments, such as aging, can significantly enhance the superelasticity and shape recovery of NiTi alloys produced via EBM, owing to the high density and controlled microstructure achievable with this method. Moreover, NiTi's intrinsic corrosion resistance and wear properties are preserved, making EBM-fabricated SMAs particularly suitable for biomedical implants and implantable devices.

However, the process's high energy density can introduce defects, such as small pores or uneven microstructures, which influence corrosion resistance and fatigue life. Zhang et al. showed that optimizing process parameters affects the defect landscape within EBM-produced NiTi, with more uniform pore distributions correlating with enhanced corrosion resistance (see Figure 4B and 4C). Precise control over the energy input, scan strategy, and preheating conditions is essential for attaining reliable, high-performance SMA parts[177,178]. The high-temperature environment in EBM also opens new possibilities for fabricating functionally graded materials and complex porous structures, which are advantageous in biomedical tissue scaffolds, orthopedic implants, and smart actuators. Its ability to produce dense, oxidation-free, and customizable NiTi components makes EBM a promising platform for personalized, high-value medical solutions and advanced aerospace components.

Dutkiewicz et al.[185] demonstrated the successful application of the EBAM method to fabricate high-quality NiTi components with a rectangular geometry. Utilizing an electron beam welding system with a wire feeder inside a vacuum chamber, NiTi wire containing approximately 50.97 at.% Ni was processed, resulting in a material characterized by columnar grains elongated along the build direction, indicative of epitaxial grain growth directly from the substrate. The AD material exhibited martensitic and reverse transformations over a temperature range from −10 to 44°C. Post-deposition aging at 500°C shifted these transformation peaks to higher temperatures and sharpened their profiles. The material demonstrated a maximum recoverable strain of approximately 3.5% when deformed along the deposition axis. When aged at 500°C for 2 hours, the alloy showed martensite formation at lower stress levels, with a gradual increase in stress at around 2.5% strain and limited shape recovery, likely due to higher martensitic transformation temperatures. In situ SEM tensile testing perpendicular to the deposition direction revealed that martensite nucleated heterogeneously at grain boundaries and surfaces, with crystallographic relationships identified between B2 and B19′ martensite phases, including (100)B2||(100)B19′ and (100)B2||(011)B19′. Fully austenitic microstructure was observed in samples aged at 500 °C, but increasing deformation induced martensite formation, predominantly with a 45° tilt relative to the tensile axis, along with the presence of type I invariant twin boundaries at higher strains. These findings highlight the capacity of EBAM to produce NiTi structures with desirable microstructural features and shape memory properties, demonstrating potential for advanced applications in smart materials and biomedical devices[185].

Otubo et al.[44] compared traditional vacuum induction melting (VIM) and innovative EBM processes for producing NiTi SMAs. While VIM using graphite crucibles introduces significant carbon contamination, up to ten times higher than EBM, EBM with water-cooled CU crucibles effectively minimizes both carbon and oxygen impurities due to operation in high vacuum. Adjustments in VIM, such as replacing graphite crucibles with low-porosity variants and increasing crucible size, can halve carbon content, yet EBM consistently achieves much lower levels, as low as 70ppm. Since contamination by carbon and oxygen directly influences the martensitic transformation temperatures, reducing them by up to 100°C, the purity of the final product is crucial, especially for biomedical applications. Ultimately, EBM proves to be a viable and superior method for producing high-purity NiTi alloys with controlled transformation properties, essential for advanced functional and medical devices[44].

Altug-Peduk et al.[187] explored the AM of NiTi SMAs via EBM, focusing on how processing conditions influence microstructure and hardness. Microstructural analyses using SEM, EDS, and XRD confirmed that the powder and bulk Ti-55% Ni components possess desired particle sizes, high packing density, and phase compositions aligning with literature; featuring austenite, martensite, and Ti_2Ni intermetallic phases. Process parameters such as scanning speed, beam current, and preheating were optimized to produce dense, well-structured samples, with XRD revealing a dominant austenitic phase and a secondary monoclinic martensite phase. Hardness measurements ranged from 264 to 417HV, indicating suitability for functional applications. Overall, EBM demonstrates a promising approach for fabricating complex NiTi components with controlled microstructures, offering significant advantages for biomedical and aerospace industries. Future investigations will focus on shape memory and superelastic behaviors of these additively manufactured alloys[187].

4.2.2 Cu-based SMAs

This section explores how the EBM process influences the microstructure and mechanical performance of Cu-based SMAs, highlighting the relationship between manufacturing parameters and final quality. Additionally, the impact of post-processing techniques, such as thermal treatments, is examined to demonstrate methods for enhancing the overall quality and performance of the printed CU-based components[188-190].

The AM of CU alloys via EBM has been extensively investigated for various applications, including non-SMA[191-196] and SMA[197-199] CU-based alloys. EBM's high energy density and rapid thermal cycles enable the fabrication of complex copper structures with tailored microstructures and enhanced properties. For example, Momeni et al.[191] examined the microstructural evolution of Cu-25Cr alloys processed by EBM, revealing a fine, heterogeneous microstructure with Cr-rich phases and sub-micron Cr spheroids embedded within the CU matrix. Ramirez et al.[192] studied the fabrication of CU reticulated meshes and open-cell foams, observing increased hardness due to Cu_2O precipitates and dislocation networks, which impede dislocation motion. Further applications include the development of intricate open-cell structures for electrical and thermal management[194], as well as catalytic structures such as high-precision Raney-Copper foams produced via dealloying[196].

CU-based SMAs also exhibit reversible shape changes and superelasticity, driven by their microstructure and phase transformations. Using AM techniques like EBM, it is possible to produce complex Cu-based SMA components with tailored properties. EBM enables precise control over microstructure and density, facilitating the development of advanced smart devices with enhanced performance. Recent advancements in the fabrication of SMAs have increasingly relied on AM technologies, such as EBM, to produce complex, precisely controlled microstructures. Hussain et al.[197] demonstrated that SMAs like TiNi, TiNiPd, and their variants exhibit unique properties such as superelasticity and SME, which are highly sensitive to microstructural features, phase transformations, and precipitate distributions. Studies have shown that AM processes, including EBM, enable the tailored development of SMA components with optimized microstructures, improved mechanical properties, and enhanced functional performance. For instance, research by Hussain et al.[197] has highlighted that incorporating alloying elements such as CU through AM techniques can significantly modify phase transformation temperatures and microstructural characteristics, leading to superior thermal stability and shape memory behavior. These developments underscore the potential of EBM not only for fabricating intricate SMA geometries but also for achieving material properties unattainable by conventional methods, thus broadening their applications in biomedical, aerospace, and actuator systems.

Gamzina et al.[198] emphasized the importance of post-processing techniques, particularly electron polishing, to enhance the surface quality of EBM CU parts. Their research indicated that electron polishing could improve the surface resolution by approximately 50%, reducing surface roughness from several tens of microns to finer scales. Additionally, their successful deposition of CU onto alumina substrates showcases the process's capability for multi-material fabrication, opening avenues for integrated device manufacturing. However, the interfaces between dissimilar materials require careful control to prevent defect formation.

4.2.3 Fe-based SMAs

EBM presents a highly promising technique for joining Fe-based SMAs. Its notable advantages include exceptional flexibility, thanks to the near-instantaneous deflection of the beam, a lower heat input compared to conventional fusion welding methods, and excellent weld seam protection provided by the vacuum environment. Consequently, this process is often selected for welding materials that are typically challenging to join[199]. For SMAs, the concentrated energy delivery ensures that microstructural modifications are confined to a small region, minimizing potential impacts on their functional properties. Despite its potential, the only available research on vacuum electron beam welding of Fe-Mn-Al-Ni has been conducted by Krooß et al.[26], who welded 5-mm-thick bars and examined the microstructural development and superelastic behavior under compression after cyclic heat treatment (CHT). Their findings indicate that the microstructure is slightly affected in the former weld zone, with grain boundaries still observable post-CHT. Importantly, no adverse effects on superelasticity under compression were detected due to the welding process.

Bauer et al.[199] demonstrated that vacuum electron beam welding provides a reliable method for joining hot-rolled Fe-Mn-Al-Ni shape memory alloy sheets, producing very narrow weld seams (less than 500μm) and minimal heat-affected zones, which helps maintain the overall integrity of the material. The study showed that by optimizing process parameters, such as preheating with an oscillating electron beam and beam oscillation during welding, cracking can be effectively minimized, even at high cooling rates. Although cyclic heat treatment can promote abnormal grain growth across the weld seam, some smaller grains tend to remain within the former weld zone regardless of welding conditions. Importantly, the functional superelastic properties are largely unaffected by the welding process because the phase transformations responsible for these properties occur mainly in the larger grains outside the weld zone, ensuring that structural failure does not originate from the weld itself.

Torrent et al.[200] conducted a study utilizing EBM to process an iron-manganese-aluminum-nickel (Fe-Mn-Al-Ni) shape memory alloy on an AISI 304 austenitic steel substrate, aiming to explore the potential for creating functionally graded structures comprising both functional and structural materials. The research involved fabricating compression specimens with equal

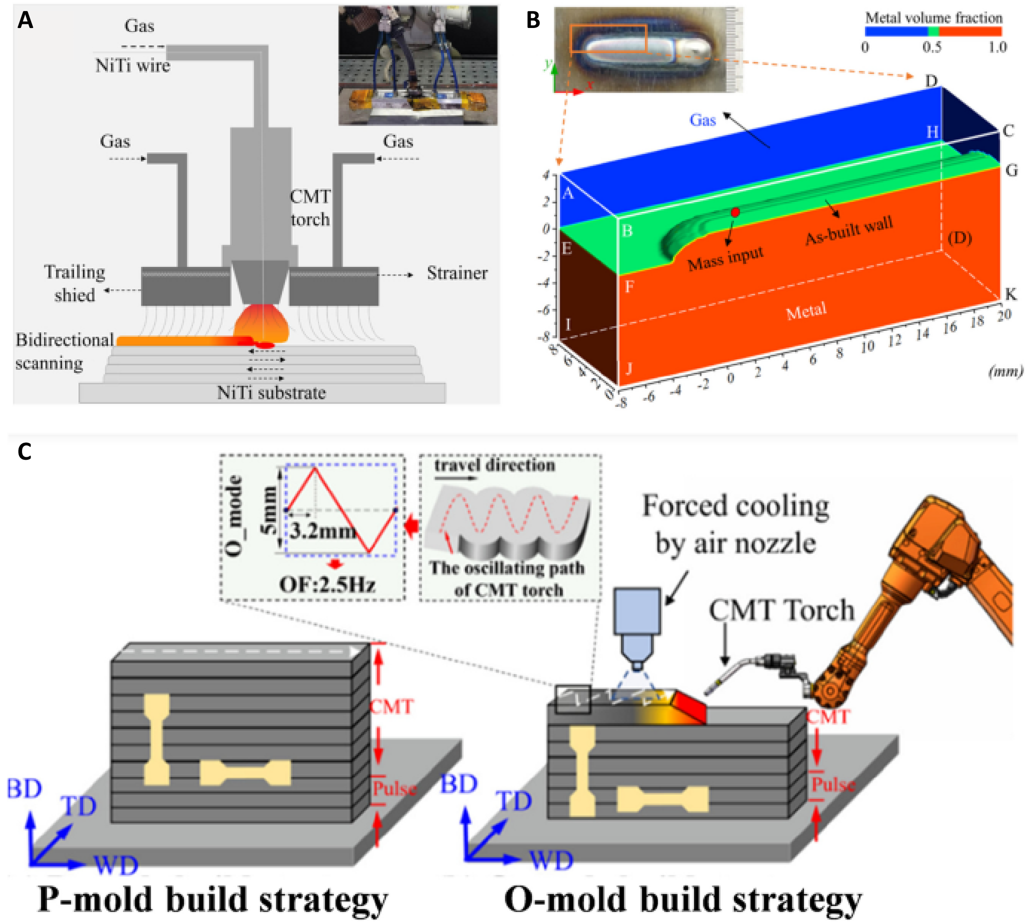

Figure 11. Schematic and Process Analysis of CMT and WAAM Strategies. (A) Illustration of the Cold Metal Transfer (CMT) mechanism in EBM processes. Reprinted with permission from Ref.[201]. (B) Diagram of the simulation model, depicting the computational domain used during the fifth layer deposition in the process. (C) Depiction of the deposition strategies and sample orientations for the WAAM-Inconel 718 wall: the parallel deposition mode (left) and the oscillating deposition mode (right). Reprinted with permission from Ref.[202].

parts of the shape memory alloy and the steel platform, followed by microstructural analysis in both the as-built state and after various heat treatments, with particular attention to the interface between the two materials. Using scanning electron microscopy and EBSD, the study revealed that the as-processed microstructure exhibits a preferred orientation aligned with the build direction. Additionally, appropriate post-processing heat treatments were shown to optimize the microstructure for enhanced pseudoelastic behavior. Mechanical performance was evaluated through incremental strain tests, applying up to 12% compression, demonstrating the material's potential for functional applications.

4.3 Wire Arc Additive Manufacturing (WAAM) for SMAs

4.3.1 NiTi-based Objects

WAAM is an innovative technique that constructs 3D metal components by sequentially melting and depositing metal wires or arcs, as illustrated in Figure 5A. This process employs controlled arc welding, such as GMAW, to fuse successive layers, offering a scalable and cost-effective route for producing large, complex-shaped SMAs[201].

WAAM's core advantage lies in its capacity to deposit high volumes of material rapidly, making it especially suitable for fabricating sizeable NiTi structures that are otherwise challenging to produce with powder-based methods. By precisely adjusting welding parameters, such as current, voltage, travel speed, and wire feed rate, manufacturers can tailor microstructure and mechanical properties to specific application needs. This flexibility enables the fabrication of components with complex geometries, including biomedical implants, aerospace parts, and adaptive mechanisms (Figure 11)[201].

Recent developments include the integration of CFD modeling to simulate molten pool dynamics and optimize processing conditions. For example, Zuo et al. employed a Ta foil-composite NiTi wire as feedstock and used in-situ arc synthesis to produce NiTiTa ternary SMA components with high geometrical accuracy and tailored microstructures[122]. Their work demonstrated that oscillating deposition modes promote better melt pool wettability, reducing overflow and defects, which is critical for achieving high-quality, functional NiTi parts.

Furthermore, the development of advanced process control strategies, incorporating real-time monitoring of temperature, arc stability, and melt pool behavior, has led to improved microstructural uniformity and minimized defects such as porosity and cracks. These enhancements translate into superior shape memory performance, including improved superelasticity and fatigue resistance.

WAAM's high deposition rate and material efficiency make it ideal for producing large-scale SMA components for aerospace, biomedical, and structural applications. Its adaptability for bioprinting remains an emerging frontier, promising the direct fabrication of patient-specific implants and tissues with complex architectures, thereby revolutionizing personalized medicine and regenerative therapies.

4.3.2 Cu-based SMAs

It is reported that Cu-based SMAs, due to their high alloying content and complex microstructural features, are particularly sensitive to thermal cycling during AM processes such as WAAM. The repeated thermal cycles are expected to influence the microstructure evolution, precipitate formation, and resultant mechanical properties, potentially leading to anisotropic behavior and internal defects. Given the nature of WAAM, which involves layer-by-layer deposition with localized high temperatures, it is anticipated that thermal accumulation will cause partial remelting of previous layers, impacting phase stability and hardness. Additionally, the formation of microcracks and porosity during rapid cooling and reheating cycles is a concern that could compromise mechanical integrity[203,204].

Al-Zn-Mg-Cu alloys are highly valued in aerospace applications due to their favorable strength-to-weight ratio and corrosion resistance[205]. WAAM offers a promising route for producing large-scale, complex metallic structures from these alloys[206-210]. However, understanding the influence of WAAM's thermal cycles on the microstructural development and mechanical performance remains limited. Yu et al.[211] systematically examined the thermal history during WAAM, quantifying the temperature profiles and their effects on microstructure evolution and mechanical behavior of the deposited Al-Zn-Mg-Cu alloy.

The thermal cycles inherent to WAAM resulted in accumulated heat within the previously deposited layers, with peak temperatures exceeding 700°C after multiple layers, notably surpassing the eutectic liquation threshold of 478°C. This repeated thermal exposure led to partial remelting of earlier layers, influencing the microstructure and mechanical properties. Microstructural analysis revealed the presence of microcracks, primarily liquation cracks, pores, and interdendritic crystalline phases, all of which contributed to a reduction in tensile strength. The tensile properties measured were approximately 300MPa in the transverse direction and 250MPa along the deposition (longitudinal) axis. The microstructure predominantly featured grains oriented at about 65° relative to the build direction, which resulted in anisotropic tensile behavior; notably, the fracture path in vertical specimens often intersected brittle η phases, $Mg(Zn,Cu,Al)_2$, further compromising mechanical integrity.

Microhardness measurements indicated a dynamic evolution correlated with the thermal history. The hardness peaked at approximately 130HV after four to seven thermal cycles, primarily due to the formation of Guinier-Preston zones, which serve as effective precipitate strengthening agents. Conversely, sustained high-temperature exposure led to a hardness reduction to around 104HV, associated with the development of fine *η′* and coarse η phases. These phases, resulting from continuous thermal cycling, significantly influenced the precipitation behavior and overall hardness profile, effectively dividing the microhardness distribution into two zones: an unstable zone characterized by phase transformations and a stable zone where the microstructure was more resistant to further changes. Overall, this study demonstrates that the thermal cycles in WAAM critically impact the microstructural features and mechanical performance of Al-Zn-Mg-Cu alloys. Controlling process parameters such as peak temperature and cooling rate is essential to mitigate adverse effects like cracking and undesirable phase coarsening, thereby enhancing the structural integrity and functional properties of additively manufactured aerospace components[211].

Al-Cu alloys offer significant potential for aerospace applications, but WAAM processing introduces challenges related to liquation cracking. Xu et al.[212] investigates the mechanisms underlying crack initiation, emphasizing microstructural evolution, grain boundary characteristics, Cu segregation, and eutectic transformations.

Macrocracks (6-9cm length, 5.6-7mm depth) predominantly occur at the bottom of the build, forming as liquation cracks along high-angle grain boundaries (30°-60°). During re-heating, temperatures surpassing 548 °C induce partial melting, transforming discontinuous eutectics into continuous divorced eutectics within grain boundaries. Microstructural analysis reveals a transition from fine grains at the fusion zone (due to high thermal gradients), to coarse columnar grains in inner layers, resulting in reduced grain boundary density and increased crack susceptibility. Solute segregation remains relatively uniform across layers, as indicated by Scheil modeling. The combination of low grain boundary density and coarse grain structure promotes the formation of wider liquid films during re-solidification, which, coupled with intergranular strains, facilitates crack initiation and propagation along high-angle boundaries. These findings highlight that liquation cracking is primarily driven by grain boundary liquid film formation in conditions of low boundary density and high strain, rather than solidification cracking[212].

Understanding these microstructural and thermal factors provides avenues for optimizing WAAM parameters, such as controlling thermal gradients and grain boundary characteristics, to mitigate cracking and enhance the reliability of additively manufactured Al-Cu aerospace components. While high-performance AM of small aluminum components is well-established, producing large-sized parts via WAAM remains challenging in achieving uniform microstructure and superior mechanical properties. Xu et al.[213] employed cold metal transfer WAAM (CMT-WAAM) to fabricate Al-5.49Cu-0.4Mn-0.29Cd (ACMC) alloy, aiming to optimize microstructure and enhance mechanical performance.

The AD samples exhibit a layered structure composed of equiaxed grains, with significant Cu-rich eutectic precipitates at grain boundaries. Microstructural stability is maintained after heat treatment, with negligible grain size variation (23μm). Heat treatment dissolves the eutectic phases, enabling Cu to enter the α-Al matrix and precipitate fine θ′ phases (100-200nm), which are uniformly distributed. The presence of Cd promotes θ′ precipitation via Cu-Cd vacancy clusters, while secondary phases such as Al_3(Ti, Zr) and micron-sized ACMF phases influence crack behavior and grain boundary stability.

Mechanical testing reveals significant improvements post heat treatment, with UTS reaching 483.7MPa, YS at 412.3MPa, and microhardness increasing from 80HV to 159HV. The primary strengthening mechanism is precipitation hardening by *θ*′ phases, which impede dislocation motion. Fracture mode transitions from intergranular in the AD state, facilitated by eutectic phase separation, to transgranular in HT samples, reflecting enhanced matrix strength and crack resistance. This work elucidates the microstructure evolution mechanisms that govern the mechanical enhancements in CMT-WAAM ACMC alloys, providing a theoretical foundation for microstructural optimization and the development of large-scale high-performance aluminum components for aerospace applications[213].

4.3.3 Iron-based SMAs

Among AM techniques, WAAM is a form of DED, utilizing an electric arc as the heat source and metal wire(s) as the material feedstock. WAAM offers economic advantages by employing commonly available equipment and raw materials widely used in welding. A substantial concentration of solute elements can create a broad freezing interval, resulting in a slow solidification process where the liquid fraction decreases gradually. As solidification concludes, a small residual liquid in the interdendritic regions can cause cracking under tensile stress, since this tiny amount of liquid cannot sustain the structural integrity of the surrounding solidified material. This phenomenon is a general principle of solidification cracking, although the specific cracking mechanisms vary depending on the alloy system and require detailed investigation for each case.

During WAAM, hot or solidification cracking can pose significant challenges, especially when depositing alloys rich in solutes such as Inconel 718. The formation of phases like Laves phase, which is influenced by the heat input during processing, often contributes to hot cracking issues. Similarly, the WAAM of functionally graded structures combining Inconel 625 and stainless steel 308L has encountered such problems, as noted by Li et al[214] .They observed that segregation of elements like niobium and molybdenum led to the formation of low-melting-point metal carbides and Laves phases at grain boundaries, causing fracture in the deposit.

Koley and Ganguly[215] conducted a study focusing on the fabrication of iron-based SMA (FeSMA) using WAAM, a form of DED. They utilized a metal powder-cored wire as the feedstock and employed a plasma-transferred arc welding torch attached to an industrial robot for the deposition process. During manufacturing, severe hot cracking was encountered, with vertical cracks developing along the build direction during the solidification of each layer. Once initiated, these cracks propagated upward through subsequent layers, making repair efforts ineffective. The cracks were closely associated with non-equilibrium secondary phases arising from intense solute segregation. Chemical analysis of these phases revealed oxygen ingress and significant solute enrichment, which contributed to an expanded solidification range and increased kinematic viscosity in the secondary phases. This broader freezing interval likely facilitated micro-crack nucleation toward the end of solidification, while the high viscosity hindered liquid flow from filling and healing these micro-defects. Additionally, residual stresses aligned along the length of the deposit, perpendicular to the cracks, promoted crack growth and coalescence, ultimately leading to embrittlement and compromised structural integrity. To address these issues, machine hammer peening was applied to each freshly deposited layer. This treatment altered the residual stress distribution, microstructural characteristics, and crystallographic texture, notably reducing the prevalence of detrimental cubic textures and increasing the proportion of low-angle grain boundaries and Σ3 boundaries. These modifications significantly enhanced the alloy's resistance to cracking and fracture.

Felice et al.[216] explored the application of FeSMAs, which are a type of smart material characterized by their shape memory and superelastic properties. Unlike other SMAs, FeSMAs are notable for their cost-effectiveness, weldability, and strong mechanical behavior, making them particularly suitable for use in the construction sector. Recognizing their potential, this study marks a pioneering effort to incorporate a Fe-Mn-Si-Cr-Ni-V-C SMA into arc-based directed energy deposition AM, specifically WAAM. The research focused on analyzing the microstructural development and the resultant mechanical and functional properties of the produced material. The WAAM-fabricated FeSMA exhibited minimal porosity and high deposition efficiency. Microstructural investigations, employing electron microscopy and high-energy synchrotron X-ray diffraction, revealed that the AD alloy predominantly consisted of the γ FCC phase, along with smaller quantities of VC, ε, and σ phases. Mechanical testing, including tensile and cyclic evaluations, demonstrated the alloy's impressive performance, with a yield strength of 472MPa, a fracture stress of 821MPa, and a fracture strain of 26%. Post-mortem synchrotron X-ray diffraction confirmed the transformation of the γ phase to the ε phase during tensile deformation leading to fracture. Furthermore, cyclic testing over 100 load/unload cycles showed stable functional behavior, indicating the material's promising potential for structural applications.

5 ADVANCED AM OF ARCHITECTED SMAS

To obtain high-quality, functional parts, the use of appropriate feedstock material is essential and often constitutes a limiting factor in fabricating complex architected components. In LPBF processes, powders must have a suitable size distribution and flowability to form a dense powder bed. This is particularly critical in lattice structures, where the density of the powder bed directly impacts the integrity of small features such as thin struts. Imperfections or insufficient density can lead to rupture during processing, compromising the entire component. Additionally, the powder must be free of excessive contaminants such as oxygen (O), nitrogen (N), and carbon (C), which can form permanent inclusions, alter transformation temperatures, and reduce fatigue life. Oxygen content is especially critical, as it tends to increase during processing; powders with larger particle sizes, like those used in DED or wire-based processes, have a lower surface-to-volume ratio and are less prone to oxidation but offer lower resolution. Conversely, the small powders used in LPBF provide finer detail but are more susceptible to oxidation, which can increase surface roughness and introduce impurities affecting the microstructure[217].

Powder contamination with oxide inclusions or impurities can lead to increased surface roughness, particularly in thin features such as lattice struts, which are sensitive to sintering anomalies. The presence of adherent or partially sintered particles can compromise mechanical performance and lead to increased roughness correlated with particle size[216]. Moreover, process parameters such as laser power, scan speed, and energy density must be carefully optimized to minimize issues such as nickel evaporation and oxygen pick-up. Excessive energy input can cause nickel loss and promote impurity absorption, distorting the transformation temperatures critical for functional properties[217]. Regulatory standards often specify that oxygen levels in the final component must be below 500ppm to ensure biocompatibility and consistent behavior[218].

Studies have demonstrated that increasing energy density during processing can elevate nickel evaporation and impurity incorporation, with even minor variations (around 0.1 atomic percent Ni) leading to temperature shifts of approximately 10°C within the material[219,220]. Conversely, elements such as C and O tend to form oxides and carbides, reducing Ti content and potentially decreasing transformation temperatures. Therefore, both feedstock quality and minimization of oxygen uptake are vital for producing reliable NiTi components, especially in biomedical applications where high surface exposure to oxidation presents additional challenges[221].

For fabricating complex lattice geometries, two main approaches are used:

Computer-aided design (CAD): Using CAD files with predefined pore geometries allows for precise control over pore size and distribution, leading to high accuracy and predictable mechanical behavior. This method is preferred for biomedical implants where pore architecture influences osseointegration and tissue growth.

Parameter-Driven Porosity: Adjusting scanning parameters, such as hatch distance, laser power, and scan orientation, during printing can induce porosity in otherwise dense structures. This approach offers higher productivity and design flexibility but results in less uniform pore geometries and irregular surfaces. For example, Habijan et al.[222] investigated such strategies by comparing parts with CAD-designed porosity against those created by process parameter variation, showing feasible porosity control but increased surface irregularities and Ni-ion release due to entrapped powders.

The advent of AM has revolutionized the fabrication of complex, architected structures from SMAs, particularly NiTi, owing to its unique thermo-mechanical properties. The capability to precisely control internal geometries enables the development of lattice architectures that exhibit tailored mechanical responses, enhanced biocompatibility, and optimized functional performance for advanced biomedical applications and smart structural components.

5.1 Material Selection and Powder Characteristics

The foundational element of successful lattice fabrication is the choice of high-purity NiTi powder, which must possess stringent specifications regarding particle size distribution, flowability, and chemical purity. Typically, powders with a particle size range of 15-45μm are employed in LPBF, providing a balance between resolution and process stability. Achieving a spherical morphology with minimal satellite particles ensures uniform flow and packing density, which are critical for fabricating defect-free lattice structures with consistent mechanical properties.

Alloys with controlled compositions, often near equiatomic NiTi, are prepared using VIM followed by gas atomization. Post-atomization heat treatments or sieving processes are employed to refine particle size and remove agglomerates, thereby reducing the likelihood of internal porosity and surface irregularities. The chemical purity, especially low levels of oxygen ($<$500ppm), is vital, as oxygen incorporation during processing can lead to the formation of brittle titanium oxides, impairing the SME and fatigue life.

5.2 AM Techniques for Lattice Fabrication

LPBF remains the predominant technique for constructing NiTi lattice architectures, owing to its ability to produce intricate geometries with micron-scale resolution. The process involves selectively melting layers of NiTi powder with a high-powered laser, following finely tuned process parameters: laser power, scan speed, hatch spacing, and layer thickness. These parameters directly influence the thermal gradients, cooling rates, and residual stresses within the build, which in turn dictate microstructure evolution and defect formation.

Alternative methods such as DED and EBM are also explored for larger-scale or functionally graded lattices. DED offers higher build rates and the possibility of in-situ alloying or compositional gradients, while EBM provides higher process stability and reduced oxidation due to the vacuum environment.

5.3 Architectural Design of Lattice Structures

Designing lattice architectures involves a dual approach: geometric parametric control and functional optimization. CAD-based models enable the precise definition of unit cell geometries, such as octahedral, diamond, or truncated cubic cells, allowing for predictable mechanical properties, controlled porosity, and tailored stiffness. These designs facilitate cellular structures with interconnected porosity, promoting tissue ingrowth, vascularization, and nutrient transport, which are essential in biomedical implants.

Alternatively, process-driven porosity generation leverages the modulation of process parameters during fabrication. By adjusting laser power and scan speed dynamically, engineers can induce controlled variations in density within the lattice, creating gradient porosity tailored to specific functional zones. While this method offers rapid prototyping advantages, it often results in less uniform pore sizes and irregular surface textures, which require post-processing for clinical-grade applications.

5.4 Microstructural Evolution and Defect Formation

The microstructure attained through AM greatly influences the functional properties of NiTi lattices. Rapid cooling rates inherent in LPBF lead to the formation of fine martensitic or R-phase microstructures, which are crucial for the SME and superelasticity. However, process-induced defects, such as lack of fusion, keyhole porosity, and gas entrapment, pose significant challenges.

Micro-CT analysis reveals that internal porosity within lattice struts can range from a few micrometers to several hundred micrometers, depending on process parameters. For instance, suboptimal laser energy input often results in incomplete melting, leaving unbonded regions or residual pores that compromise mechanical integrity. Conversely, excessive energy induces keyhole porosity, spherical voids caused by vaporization; reducing fatigue life and altering transformation behavior.

Optimizing the energy density, often expressed as E=P/(v×h)E=P/(v\times h)E=P/(v×h), where PPP is laser power, vvv is scan speed, and hhh is hatch spacing, is critical. For NiTi, studies have shown that energy densities in the range of 50-80J/mm^3 promote dense, well-bonded microstructures with minimal porosity, whereas deviations outside this window increase defect prevalence.

5.5 Microstructural Control and Phase Transformation

The microstructure within NiTi lattice structures influences their shape memory and superelastic behavior. Rapid cooling during LPBF promotes a predominantly martensitic microstructure at room temperature, which can be further manipulated through post-process heat treatments. Solution annealing and aging can stabilize austenite or martensite phases, tuning the transformation temperatures (MsM_sMs, AsA_sAs) to desired levels for specific applications.

The phase transformation behavior is sensitive to residual stresses, grain size, and impurity levels. For example, residual stresses introduced during rapid cooling can shift transformation temperatures, affecting actuation performance. Similarly, oxygen contamination can precipitate Ti oxides that act as stress concentrators, reducing fatigue strength. Thus, precise control over process atmosphere (preferably inert or vacuum), powder chemistry, and thermal post-treatments is essential.

5.6 Mechanical Performance and Functional Testing

The mechanical response of NiTi lattice structures is characterized by a combination of elastic deformation, phase transformation, and plasticity. Their superelasticity enables large recoverable strains (>6%), making them suitable for load-bearing implants and actuators. Finite element modeling, coupled with experimental validation, guides the optimization of unit cell geometry and strut dimensions to balance stiffness, strength, and damping.

Fatigue testing under cyclic thermomechanical loading reveals that defect density, surface roughness, and residual stresses are critical factors influencing durability. For biomedical devices, long-term stability under physiological conditions requires rigorous testing, including corrosion resistance assessments and biocompatibility evaluations.

The integration of computational topology optimization with AM techniques paves the way for next-generation NiTi lattice structures with hierarchical porosity and multiscale functionalities. AM's ability to produce patient-specific implants with complex internal architectures opens new horizons in personalized medicine.

However, challenges remain in achieving consistent microstructure control, minimizing defects, and scaling up production while maintaining rigorous quality standards. Innovations in process monitoring, in-situ feedback control, and advanced post-processing treatments are vital to fully harness the potential of architected SMAs fabricated via AM.

6 GEOMETRICAL QUALIFICATION

6.1 Internal Defects

Additively manufactured parts often contain defects related to powder quality and process parameters. The most common issues include lack of fusion, porosity, and gas entrapment, which can be detected via micro-CT scanning. Studies by Gustmann et al.[223] and Biffi et al.[224,225] utilized micro-CT to analyze 3D-printed NiTi lattice samples, revealing that porosity within diamond-like lattice structures ranged from 30μm to 250μm, with defect sphericity ratios between 0.45 and 0.7. Homogeneous defect distribution was achievable through optimized scanning strategies. The shape and size of internal pores are strongly influenced by process parameters: insufficient energy results in low sphericity and incomplete fusion, while excessive energy induces spherical pores due to gas entrapment. Yang et al.[226] further assessed defect formation across different strut diameters and scanning velocities, observing that defects tend to concentrate at nodes, with diameters limited to less than 0.2mm. Lower scanning speeds (e.g., 200mm/s) reduced defect quantity, whereas higher speeds (e.g., 800mm/s) increased defect size and number, especially in finer structures.

6.2 Dimensional Qualification

Beyond internal defects, process-induced geometrical deviations such as distortion and dimensional inaccuracies impact the performance of lattice structures, especially in biomedical applications where fit and function are critical. The accuracy of LPBF parts depends on laser spot size, layer thickness, scan speed, and thermal behavior, often described through volumetric energy density equations, such as:

E=Pv×hE=\frac{P}{v \times h}E=v×hP

where PPP is laser power, vvv is scan speed, and hhh is hatch spacing. Variations in these parameters influence the final geometry, surface quality, and microstructure.

Studies indicate that higher laser power can cause over-melting, leading to thicker struts and dimensional mismatches. For instance, Dadbakhsh et al.[227] fabricated NiTi porous scaffolds with octahedral units at different laser powers, finding that high power (250W) caused up to 71.8% mismatch in strut thickness, whereas low power (40W) minimized deviation (~15.6%). Despite better dimensional accuracy, low power settings may produce less dense structures, necessitating a balance between density and geometric fidelity[227]. Orientation during building also influences dimensional accuracy; perpendicular walls tend to accumulate larger particles due to partially melted powders, affecting surface roughness and feature fidelity. Adjusting process parameters, particularly laser power and scan speed, can optimize this balance. For example, reduced laser power combined with slower scan speeds may produce smoother surfaces and more accurate features, although at the cost of potential lack of fusion or lower density.

6.3 Surface Finishing and Roughness

Surface roughness inherently exceeds that of ideal models in LPBF-fabricated parts, especially in lattice structures with high surface area exposure. Roughness levels are categorized as smooth (<0.5μm), minimally rough (~0.5-1μm), moderately rough (>1-2μm), and rough (>2μm). Increased roughness can benefit bone cell attachment but negatively impact mechanical strength and biocompatibility due to higher ion release and inflammation risk[228].

Post-processing techniques such as chemical etching, electropolishing, laser polishing, and abrasive methods are routinely employed to reduce roughness.

Electropolishing effectively removes unmelted particles but can also thin the struts, potentially affecting mechanical properties and transformation behavior[229]. Surface treatments must be carefully tuned; for example, a 7-minute HF/HNO_3 treatment successfully removes residual powders while preserving structural integrity[228].

In biomedical applications like vascular stents, a smooth surface is essential to prevent blood flow damage and thrombosis. Surface finishing methods, such as acid etching and sandblasting, have demonstrated significant roughness reductions, from values around 7.17μm to approximately 0.34μm[230]. Additionally, surface finishing enhances the accuracy of numerical models by reducing variable cross-sections and micro-roughness, enabling more reliable simulations of mechanical and biological performance.

7 APPLICATIONS OF LASER-PRINTED SMAS

7.1 Biomedical Devices

3D-printed SMAs are increasingly recognized for their transformative potential in orthopedics. Their intrinsic SME allows implants to dynamically conform to changing bone structures during healing, promoting superior integration and biocompatibility. Such adaptability paves the way for innovative solutions in fracture stabilization and bone defect reconstruction. For instance, Hamann et al. employed LPBF to integrate NiTi SMA sheets with additively manufactured Ti-6Al-4V frameworks, creating hybrid pedicle screws with functional capabilities[231]. Similarly, Jahadakbar et al. utilized 3D printing to develop NiTi-based fixation plates with tunable stiffness and geometries tailored for specific surgical needs, subsequently validating their mechanical performance through experimental testing[232]. Further, by optimizing processing parameters and incorporating engineered porosity, Jahadakbar's team successfully produced superelastic, porous NiTi structures with stiffness closely approximating that of cortical bone, enabling more personalized and resilient fixation devices in mandibuloplasty[233]. Despite these promising developments, several hurdles remain, chiefly, ensuring the biocompatibility of these alloys, their long-term stability within the body, and precise control over their shape-changing behavior. Addressing these challenges is critical for translating 3D-printed SMAs into widespread clinical use, ultimately offering more innovative, patient-specific solutions for bone repair.

Although NiTi alloys remain the cornerstone of many biomedical applications due to their superior biocompatibility, corrosion resistance, and unique shape memory and superelastic properties, recent research has expanded into alternative SMA systems where biocompatibility constraints are less stringent. In particular, CU-based SMAs have garnered interest for their distinct mechanical and functional characteristics, especially in applications where biocompatibility is not the primary concern.

For instance, single-crystal Cu-Al-Ni alloys are being investigated for their potential as actuators within anthropomorphic upper limb prosthetic devices[234]. These alloys offer advantageous properties such as rapid response times, significant deformation capabilities, and ease of fabrication, making them suitable for dynamic actuation in complex prosthetic systems.

Beyond prosthetic actuators, Cu-based SMAs like Cu-Al-Be are also being explored within the field of dental medicine, particularly for endodontic tools. These alloys exhibit promising mechanical attributes for procedures such as root canal preparation, where flexibility, resistance to cyclic fatigue, and precise cutting ability are critical. Comparative studies have shown that Cu-Al-Be alloys can achieve penetration depths comparable to, or even exceeding, those of NiTi-based instruments, with the added benefit of antimicrobial activity. This antimicrobial property offers a dual function, facilitating mechanical debridement while actively reducing microbial load, thereby enhancing treatment efficacy[235,236].

Furthermore, Cu-Al-Be alloys demonstrate the ability to inhibit biofilm formation and assist in smear layer removal, which are crucial steps in endodontic therapy. These additional functionalities could lead to the development of multifunctional endodontic instruments that not only perform mechanical tasks but also contribute to antimicrobial defense, potentially reducing the risk of reinfection and improving patient outcomes. Despite these promising applications, the use of CU-based SMAs in biomedical contexts is still in the exploratory phase. Challenges such as potential cytotoxicity, long-term stability, and corrosion susceptibility need to be carefully addressed through surface modifications and alloy optimization. Nevertheless, ongoing research continues to unveil the broad potential of CU-based SMAs in specialized biomedical fields where their unique properties can be harnessed for innovative therapeutic and functional solutions.

The application of 3D-printed SMAs in fabricating vascular scaffolds offers distinct advantages over traditional manufacturing methods. Conventional techniques such as filament winding, photochemical etching, injection molding, and laser cutting often encounter limitations, including weld seam imperfections, structural fragility, and environmental concerns like toxic gas emissions. In contrast, AM enables highly precise and customizable molding of complex scaffold geometries, overcoming these issues. This precision allows for the fabrication of intricate, small-scale structures with superior consistency and mechanical reliability. For example, Demir et al. utilized SLM to produce CoCr alloy cardiovascular stents, thoroughly characterizing their morphology and surface properties post-fabrication and electrochemical polishing[237]. Such approaches demonstrate the feasibility of replacing conventional microfabrication methods with more flexible, efficient, and accurate processes. Nonetheless, challenges such as high production costs, corrosion resistance, biocompatibility, and material tunability persist. Continued research and technological innovations are essential to overcoming these limitations and advancing SMA-based vascular scaffolds toward clinical application.

CU-based SMAs are generally limited to applications that do not involve direct implantation, such as temporary devices or external components, where the potential release of copper ions poses minimal health risks. These alloys offer notable benefits, including cost-effectiveness, quick actuation, and inherent antimicrobial effects, making them suitable for use in surface coatings, external prosthetic devices, or sterilizable instruments that do not contact tissues directly. Recent advancements in surface treatment techniques and alloy formulation have demonstrated that it is possible to significantly decrease copper ion leaching, which could pave the way for safer use of Cu-based SMAs in more controlled biomedical environments in the future. To address Cu-SMA cytotoxicity, there are several strategies show promise, including surface modifications by oxide layers (e.g., TiO_2) or polymer coatings (e.g., parylene) reduce ion diffusion by >90%[238,239], alloying through adding Ti or Zr improves corrosion resistance by forming passive films[239,240], process optimization, in which LPBF's fine grain structures decrease galvanic corrosion rates compared to cast Cu-SMAs[239].

While Cu-based SMAs are known for their beneficial properties in biomedical applications, their biocompatibility is carefully managed through design strategies such as limited exposure, encapsulation, and the use of single-use devices, which collectively mitigate cytotoxicity risks and ensure safe functionality within specific biomedical contexts. For example, regarding the dental tools, Cu-Al-Be's antimicrobial properties are exploited in endodontic files or orthodontic archwires, where short-term exposure and sterilization protocols limit cytotoxicity risks[241,242]. Single-use designs further mitigate leaching concerns. Moreover, concerning prosthetic actuators, in the external prosthetic limbs, Cu-Al-Ni actuators avoid tissue contact while providing high-force actuation. Encapsulation in biocompatible polymers (e.g., polyether ether ketone or PEEK) isolates Cu from bodily fluids[18]. In the case of biosensors, Cu-SMAs are used in fiber-optic or wearable sensors where coatings (e.g., SiO_2) prevent ion release. Their electrical conductivity enables real-time monitoring without implantation[238,239,243-245].

7.2 SMAs in Biosensing Technologies

The unique properties of SMAs make them promising candidates for biosensing applications. Their ability to undergo reversible shape transformations triggered by temperature changes offers a high degree of control and precision in sensor design. Additionally, their excellent elasticity and durability enable sensors to perform consistent performance over multiple cycles, extending operational lifespan. Furthermore, the capacity to miniaturize SMA components allows for the development of highly sensitive, minimally invasive biosensors capable of monitoring biological parameters in vivo. For example, Srivastava et al. designed SMA-based actuators for non-invasive bone diagnostics and damage assessment, employing impedance analysis to track healing processes[246]. Their non-bonded piezoelectric sensors demonstrated reduced tissue damage and more stable signals compared to bonded counterparts. However, the application of SMAs in biosensing remains in nascent stages, with challenges such as relatively slow response times, and the need for enhanced biocompatibility and corrosion resistance to ensure safe, long-term operation within biological environments.

CU-based SMAs, distinguished by their exceptional thermomechanical characteristics and their capacity to undergo reversible phase transformations, are increasingly being explored for innovative applications in sensing technologies and electronic devices. Their unique ability to respond predictably to thermal stimuli makes them promising candidates for developing highly sensitive and reliable sensors. For instance, an advanced study introduced a fiber optic sensor coated with a Cu-Al-Ni SMA layer. This sensor exhibited remarkable durability, maintaining stable performance over more than 5,000 operational cycles. Its optical response was highly precise, demonstrating the potential for deployment in smart manufacturing environments where reliability and repeatability are critical. Moreover, this fiber optic sensor showcased an extensive temperature detection range, spanning from -200°C to 300°C, and was effective in both contact and non-contact measurement modes. Notably, the sensor's sensing range could be fine-tuned by adjusting the SMA's phase transition (switching) temperature, offering customizable thermal sensitivity for diverse industrial applications[246].

In another innovative application, Cu-Al-Mn SMAs were employed in the fabrication of Schottky diodes, where they served as the Schottky contact interface on a p-type silicon substrate. These diodes demonstrated a remarkable sensitivity to incident light, effectively functioning as photodiodes. Their behavior was frequency-dependent, revealing promising capabilities for integration into optoelectronic systems. Such characteristics suggest that Cu-Al-Mn SMA-based diodes could be harnessed for advanced light detection and signal processing tasks within next-generation electronic and photonic devices[246]. The versatility of CU-based SMAs in these contexts stems from their ability to transduce thermal or optical stimuli into electrical signals, paving the way for their incorporation into smart sensors, adaptive electronics, and integrated optoelectronic systems. As research continues, these materials may unlock a new realm of multifunctional devices that combine mechanical adaptability with electronic responsiveness, broadening the horizons of sensor technology and electronics.

7.3 Actuators

Among the most prevalent applications of CU-based SMAs lies their role as actuators, primarily owing to their distinctive thermoelastic properties. When exposed to thermal stimuli, these materials can undergo reversible phase transformations that generate mechanical work, enabling precise actuation. SMA actuators are generally classified into three primary categories: (1) force actuators, which exert substantial force across extensive ranges of motion over multiple cycles; (2) proportional control actuators, which utilize partial shape recovery to achieve accurate positional control; and (3) two-way-effect actuators, capable of producing bidirectional motion to counteract external forces[247].

Despite their promising attributes, such as elevated actuation temperatures, larger displacement capacities, and lower energy requirements, research into CU-based SMAs as practical actuators remains relatively limited. Notably, alloys like Cu-Al-Ni-Mn exhibit rapid phase transformation responses at temperatures exceeding 150°C, with displacement capabilities surpassing those of comparable NiTi-based systems under similar thermal conditions. These alloys also demonstrate a lower power consumption profile, making them attractive for high-precision micro-actuation tasks such as micrograppers, micro-positioning devices, and other miniature systems[248,249]. For example, Muralidharan et al.[243] illustrated a conceptual design of an SMA/Kapton composite belt actuator fabricated via flash evaporation and integrated within a custom belt drive system inside a vacuum chamber. This configuration exhibits high displacement, substantial recovery ratios, and load-bearing capacity, rendering it suitable for high-precision platforms such as Stewart mechanisms. Additionally, in a study by Muralidharan et al., a bimorph actuator composed of a flexible polyimide substrate with a Cu-Al-Ni-Mn thin film deposited through thermal evaporation was developed. Results indicated that increasing substrate thickness to 75μm significantly enhanced performance, with the actuator operating reliably under varying loads (30mg, 45mg, and 60mg). These systems show potential for integration into Micro-Electro-Mechanical Systems (MEMS)[250].

Although CU alloys offer specific advantages, such as higher operational temperatures and greater displacement, most commercially available SMA actuators remain based on NiTi due to their well-established reliability and comprehensive understanding of their properties. For example, a high-torque NiTi-based actuator capable of delivering up to 75Nm has been reported, demonstrating the maturity of NiTi systems in demanding applications[251]. Furthermore, research by Wongweerayoot et al. showcased NiTi-CU composite actuators used in high-precision micro grippers designed for delicate objects, such as grasping and holding small plastic spheres, highlighting their potential in robotic manipulations, including humanoid robotic arms and dexterous automation[252].

7.4 Damping Devices

Seismic events pose a significant threat to structural integrity, often resulting in catastrophic damage due to intense vibrations. Consequently, the development of efficient vibration mitigation systems is crucial for civil and mechanical engineering. While NiTi-based SMAs have been extensively employed in damping applications thanks to their high energy dissipation, fatigue resistance, and superelasticity, their high costs and complex processing requirements have limited widespread adoption. Conversely, Cu-based SMAs emerge as a cost-effective and practical alternative, offering favorable mechanical properties combined with ease of manufacturing, making them suitable for a broad array of damping solutions[253-255].

Structural bracing systems are fundamental in maintaining lateral stability against wind and seismic forces, and recent investigations have demonstrated the effectiveness of CU SMA-based bracing methods. For example, Cu-Al-Be SMA wires with a diameter of 0.5 mm were integrated into the bracing elements of a scaled three-story steel rigid frame model. Results indicated significant improvements in damping capacity and energy dissipation, thereby enhancing overall structural performance during dynamic loading[256,257].

Seismic isolation techniques further leverage the energy dissipation properties of SMAs to protect structures from ground motion. Conventional isolators, such as rubber bearings and sliding bearings, are complemented by SMA-based isolators, using Cu alloys and NiTi SMAs, due to their superelasticity, fatigue durability, and excellent energy absorption. These devices are strategically positioned between critical structural components, such as girders, bent caps, or foundation levels, to attenuate seismic vibrations. For instance, shaking table experiments on structures equipped with Cu-Al-Be SMA dampers revealed a remarkable increase in damping ratios, from 0.59 to 5.95%, along with enhanced stiffness and significant reductions in peak accelerations and displacements during simulated seismic events[256]. Likewise, the placement of Cu-Al-Mn SMA elements within reinforced concrete beams has been shown to improve structural strength, rigidity, and energy dissipation capacity[258]. Prototype quasi-zero-stiffness isolators fabricated with Cu-Al-Mn SMAs further demonstrated their capacity to reduce seismic accelerations from 1.0g to approximately 0.2g, with predicted resonances around 0.6Hz, thus highlighting their potential in seismic mitigation strategies[259]. In summary, CU-based SMAs present a promising, cost-efficient avenue for developing advanced damping and seismic isolation systems, offering durable, fatigue-resistant, and highly energy-dissipative solutions suitable for safeguarding critical infrastructure against seismic hazards.

8 CONCLUSION AND FUTURE SCOPE

The integration of cutting-edge laser-based AM technologies with the inherently versatile and multifunctional nature of SMAs heralds a new paradigm in the design and fabrication of smart, adaptive systems. The precise layer-by-layer control afforded by techniques such as SLM, EBM, and wire arc AM has enabled unprecedented microstructural tailoring, allowing for the manipulation of phase transformation temperatures, microstructural refinement, and the development of architected porous and lattice structures that optimize mechanical, thermomechanical, and functional properties. These advancements have facilitated the realization of complex geometries previously unattainable through conventional manufacturing routes, thereby unlocking new potential in biomedical devices, such as patient-specific implants with integrated porosity for tissue ingrowth, as well as aerospace components capable of adaptive morphing, vibration damping, and energy absorption. The ability to engineer microstructures with controlled dislocation densities, grain orientations, and phase distributions—coupled with in-situ process monitoring, provides a pathway towards highly reproducible, defect-minimized, and performance-optimized SMA parts suitable for critical applications.

Nevertheless, the journey from laboratory proof-of-concept to industrial realization necessitates addressing several fundamental challenges. The high thermal gradients intrinsic to laser and EBM processes often lead to residual stresses and microstructural heterogeneity, which can impair fatigue performance and long-term stability. The formation of porosity, cracks, and impurity inclusions, particularly oxygen and carbon, remains a persistent obstacle, especially when fabricating intricate architectures with small feature sizes or porous networks. Achieving consistent control over these defects requires not only the refinement of process parameters but also the development of real-time, in-situ sensing and feedback systems capable of dynamically adjusting energy input, scan strategies, and thermal management. Advanced computational modelling, encompassing phase-field simulations, finite element analysis, and thermomechanical prediction, must be integrated into process development to better understand and manipulate microstructure evolution, phase stability, and transformation behavior under complex thermal histories.

Looking ahead, the future landscape of SMA 3D printing will benefit from the design of novel alloy systems, including high-entropy and multicomponent SMAs, which promise enhanced functional stability, fatigue resistance, and biocompatibility. The exploration of post-processing treatments, such as targeted heat treatments, surface passivation, and surface texturing, will be crucial in mitigating residual stresses, improving corrosion resistance, and tailoring surface properties for specific applications. Furthermore, scalable manufacturing strategies that harmonize with quality assurance protocols, including non-destructive evaluation and microstructural characterization, are essential for transitioning these materials from experimental prototypes to reliable, high-throughput production lines.

In addition, embracing the synergistic development of architected microstructures alongside advanced alloy formulations will enable the creation of multifunctional components capable of simultaneous actuation, damping, sensing, and energy harvesting. Such integrated systems could revolutionize fields ranging from minimally invasive biomedical implants and tissue engineering scaffolds to morphing aerospace structures and adaptive energy systems. As research endeavors continue to deepen in understanding the microstructure-property-process relationships, and as technological innovations converge with material science, the horizon expands toward truly intelligent, durable, and customizable SMA components. This trajectory holds the promise of transforming AM into a cornerstone of next-generation smart materials engineering, delivering solutions that seamlessly blend functionality, reliability, and scalability for the most demanding applications across industry and society.

Acknowledgements

Not applicable.

Conflicts of Interest

The authors declared no conflict of interest.

Author Contribution

Kashi PA contributed to writing–original draft, methodology, investigation, funding acquisition, and conceptualization; Didari M contributed to writing–original draft, validation, and formal analysis; Shahbaz M contributed to writing–original draft, software, resources, and methodology.

Data Availability

Data sharing is not applicable to this review as no datasets were generated or analyzed during the current study.

Abbreviation List

ACMC, Al-5.49Cu-0.4Mn-0.29Cd
AD, As-deposited
Af, Austenite finish temperature
AM, Additive manufacturing
BCC, Body-centered cubic
BD, Building direction
CAD, Computer-aided design
CMT-WAAM, Cold metal transfer waam
DED, Direct energy deposition
DMLS, Direct metal laser sintering
EBM, Electron beam melting
EBSD, Electron backscatter diffraction
FCC, Face-centered cubic
FeSMA, Iron-based shape memory alloys
GMAW, Gas metal arc welding
HEAs, High-entropy alloys
HIP, Hot isostatic pressing
HIP, Hot isostatic pressing
HT, Heat-treated
LPBF, Laser powder bed fusion
NiTi, Nickel-titanium
PM, Powder metallurgy
SAED, Selected area electron diffraction
SE, Superelasticity
SEM, Scanning electron microscope
SIM, Stress-induced martensite
SLM, Selective laser melting
SLM, Selective laser melting
SLS, Selective laser sintering
SMAs, Shape memory alloys
SME, Shape memory effect
VIM, Vacuum induction melting
WAAM, Wire arc additive manufacturing

References

[1] Sabahi N, Chen W, Wang CH et al. A review on additive manufacturing of shape-memory materials for biomedical applications. *JOM*, 2020; 72: 1229-1253.[DOI]

[2] Alagha AN, Hussain S, Zaki W. Additive manufacturing of shape memory alloys: A review with emphasis on powder bed systems. *Mater Des*, 2021; 204: 109654.[DOI]

[3] Hou H, Simsek E, Ma T et al. Fatigue-resistant high-performance elastocaloric materials made by additive manufacturing. *Science*, 2019; 366: 1116-1121.[DOI]

[4] Xue L, Atli KC, Picak S et al. Controlling martensitic transformation characteristics in defect-free NiTi shape memory alloys fabricated using laser powder bed fusion and a process optimization framework. *Acta Mater*, 2021; 215: 117017.[DOI]

[5] Parvizi S, Hashemi SM, Asgarinia F et al. Effective parameters on the final properties of NiTi-based alloys manufactured by powder metallurgy methods: A review. *Prog Mater Sci*, 2021; 117: 100739.[DOI]

[6] Shaw JA, Kyriakides S. Thermomechanical aspects of NiTi. *J Mech Phys Solids*, 1995; 43: 1243-1281.[DOI]

[7] Wen S, Gan J, Li F et al. Research status and prospect of additive manufactured nickel-titanium shape memory alloys. *Materials*, 2021; 14: 4496.[DOI]

[8] Balasubramanian M, Srimath R, Vignesh L et al. Application of shape memory alloys in engineering - A review. *J Phys Conf Ser*, 2021; 2054: 012078.[DOI]

[9] Saud SN, Hamzah E, Abubakar T et al. Microstructure and corrosion behaviour of Cu-Al-Ni shape memory alloys with Ag nanoparticles. *Mater Corros*, 2015; 66: 527-534.[DOI]

[10] Xu JW. Effects of Gd addition on microstructure and shape memory effect of Cu-Zn-Al alloy. *J Alloys Compd*, 2008; 448: 331-335.[DOI]

[11] Seok S, Onal CD, Cho KJ et al. Meshworm: a peristaltic soft robot with antagonistic nickel titanium coil actuators. *IEEE/ASME Trans Mechatron*, 2012; 18: 1485-1497.[DOI]

[12] Bhagyaraj J, Ramaiah KV, Saikrishna CN et al. Behavior and effect of Ti2Ni phase during processing of NiTi shape memory alloy wire from cast ingot. *J Alloys Compd*, 2013; 581: 344-351.[DOI]

[13] Zeng Z, Cong BQ, Oliveira JP et al. Wire and arc additive manufacturing of a Ni-rich NiTi shape memory alloy: Microstructure and mechanical properties. *Addit Manuf*, 2020; 32: 101051.[DOI]

[14] Janke L, Czaderski C, Motavalli M et al. Applications of shape memory alloys in civil engineering structures—Overview, limits and new ideas. *Mater Struct*, 2005; 38: 578-592.[DOI]

[15] Kim DH, Lee MG, Kim B et al. A superelastic alloy microgripper with embedded electromagnetic actuators and piezoelectric force sensors: a numerical and experimental study. Smart *Mater Struct*, 2005; 14: 1265.[DOI]

[16] Tomozawa M, Kim HY, Miyazaki S. Shape memory behavior and internal structure of Ti–Ni–Cu shape memory alloy thin films and their application for microactuators. *Acta Mater*, 2009; 57: 441-452.[DOI]

[17] Dora TRK, Sampath V, Li Y et al. In vitro cytotoxicity and corrosion studies of some copper base shape memory alloys. *Mater Today Proc*, 2017; 4: 10672-10681.[DOI]

[18] Čolić M, Rudolf R, Stamenković D et al. Relationship between microstructure, cytotoxicity and corrosion properties of a Cu-Al-Ni shape memory alloy. *Acta Biomater*, 2010; 6: 308-317.[DOI]

[19] Ma Y, Yan J, Yan T et al. Biological properties of Cu-bearing and Ag-bearing titanium-based alloys and their surface modifications: A review of antibacterial aspect. *Front Mater*, 2022; 9: 999794.[DOI]

[20] Jhou WT, Wang C, Ii S et al. TiNiCuAg shape memory alloy films for biomedical applications. *J Alloys Compd*, 2018; 738: 336-344.[DOI]

[21] Pereira T, Kennedy JV, Potgieter J. A comparison of traditional manufacturing vs additive manufacturing, the best method for the job. *Procedia Manuf*, 2019; 30: 11-18.[DOI]

[22] Luo J, Ye WJ, Ma XX et al. The evolution and effects of second phase particles during hot extrusion and re-extrusion of a NiTi shape memory alloy. *J Alloys Compd*, 2018; 735: 1145-1151.[DOI]

[23] Qiang X, Chen L, Jiang X. Achievements and perspectives on Fe-based shape memory alloys for rehabilitation of reinforced concrete bridges: an overview. *Materials*, 2022; 15: 8089.[DOI]

[24] Chua CK, Wong CH, Yeong WY. Standards, Quality Control, and Measurement Sciences in 3D Printing and Additive Manufacturing. Academic Press, 2017.[DOI]

[25] Dzogbewu TC. Laser powder bed fusion of Ti6Al4V lattice structures and their applications. *J Met Mater Miner*, 2020; 30: 68-78.[DOI]

[26] Li BY, Rong LJ, Li YY et al. Synthesis of porous Ni-Ti shape-memory alloys by self-propagating high-temperature synthesis: reaction mechanism and anisotropy in pore structure. *Acta Mater*, 2000; 48: 3895-3904.[DOI]

[27] Biswas A. Porous NiTi by thermal explosion mode of SHS:

processing, mechanism and generation of single phase microstructure. *Acta Mater*, 2005; 53: 1415-1425.[DOI]

[28] Dzogbewu TC, de Beer DJ, du Preez WB. Laser powder bed fusion of Ti15Mo fused tracks and layers. *JOM*, 2023; 75: 3183-3196.[DOI]

[29] Dzogbewu TC, Fianko SK, Amoah N et al. Additive manufacturing in South Africa: critical success factors. *Heliyon*, 2022; 8: e11852.[DOI]

[30] Chibinyani MI, Dzogbewu TC, Maringa M et al. Reduced order topology optimisation of a planar honeycomb defined by a linear elastic Ti6Al4V (ELI) material model. *S Afr J Ind Eng*, 2022; 33: 299-317.[DOI]

[31] Ataee A, Li Y, Brandt M et al. Ultrahigh-strength titanium gyroid scaffolds manufactured by selective laser melting (SLM) for bone implant applications. *Acta Mater*, 2018; 158: 354-368.[DOI]

[32] Hou M, Gu Q, Yang Z et al. Enhancing shape memory properties of 3D-printed NiTi alloys by laser powder bed fusion through microstructural control. *J Alloys Compd*, 2025; 1010: 178029.[DOI]

[33] Yang S, Zhang J, Peng C et al. Laser powder bed fusion of sinusoidal lattice structure using shape memory alloys. *Adv Eng Mater*, 2024; 26: 2400177.[DOI]

[34] Ba Y, Lv Y, Yan M et al. Effect of energy density on mechanical properties of NiTiCu shape memory alloys prepared by SLM. *Materials*, 2024; 17: 5693.[DOI]

[35] Lin Z, Liu Y, Liu Y et al. Study on shape memory effect and superelasticity of laser powder bed melting NiTi-Nb alloys. *Mater Sci Eng A*, 2025; 928: 148949.[DOI]

[36] Dabbaghi H, Taheri Andani N, Pourshams M et al. Processability and material behavior of NiTi shape memory alloys using wire laser-directed energy deposition (WL-DED). *J Manuf Mater Process*, 2025; 9: 15.[DOI]

[37] Zuo X, Zhang W, Chen Y et al. Wire-based directed energy deposition of NiTiTa shape memory alloys: microstructure, phase transformation, electrochemistry, X-ray visibility and mechanical properties. *Addit Manuf*, 2022; 59: 103115.[DOI]

[38] Pu Z, Du D, Chen C et al. In-situ synthesis of NiTi shape memory alloys with tunable chemical composition and thermomechanical response by dual-wire-feed electron beam directed energy deposition. *J Mater Sci Technol*, 2025; 216: 209-225.[DOI]

[39] Hamilton RF, Bimber BA, Andani MT et al. Multi-scale shape memory effect recovery in NiTi alloys additive manufactured by selective laser melting and laser directed energy deposition. *J Mater Process Technol*, 2017; 250: 55-64.[DOI]

[40] Wang F, Li M, Zhang Y et al. Laser directed energy deposition of NiTi shape memory alloys with herringbone grain architectures for enhanced ductility and superelasticity. *Mater Des*, 2025; 244: 115355.[DOI]

[41] Chen L, Oliveira JP, Yan X et al. Microstructure and phase transformation behavior of NiTiCu shape memory alloys produced using twin-wire arc additive manufacturing. *Addit Manuf* Front, 2024; 3: 200132.[DOI]

[42] Chen L, Zhao M, Wu J et al. Mechanical property strengthening by post-heat treatments in NiTiCu shape memory alloys fabricated by twin-wire arc additive manufacturing. *Virtual Phys Prototyp*, 2025; 20: e2457579.[DOI]

[43] Gonela KK, Vijayavarman C, Palanivel M et al. Effect of robotic weaving motion on mechanical and microstructural characteristics of wire arc additively manufactured NiTi shape memory alloy. *Int J Mater Res*, 2023; 114: 947-954.[DOI]

[44] Zhou Q, Hayat MD, Chen G et al. Selective electron beam melting of NiTi: Microstructure, phase transformation and mechanical properties. *Materials Sci Eng A*, 2019; 744: 290-298.[DOI]

[45] Zhang L, Ren D, Ji H et al. Study on the corrosion behavior of NiTi shape memory alloys fabricated by electron beam melting. *NPJ Mater Degrad*, 2022; 6: 79.[DOI]

[46] Dzogbewu TC, du Preez WB. Additive manufacturing of Ti-based intermetallic alloys: A review and conceptualization of a next-generation machine. *Materials*, 2021; 14: 4317.[DOI]

[47] Chernyshikhin SV, Zherebtsov DD, Fedorenko LV et al. Tailoring the functional properties of NiTi shape memory alloy by laser powder bed fusion process conditions for 4D printing. *J Manuf Mater Process*, 2025; 9: 385.[DOI]

[48] Xi R, Jiang H, Li G et al. Effect of solution treatment on the microstructure, phase transformation behavior and functional properties of NiTiNb ternary shape memory alloys fabricated via laser powder bed fusion in-situ alloying. Int *J Extreme Manuf*, 2024; 6: 045002.[DOI]

[49] Yuan B, Ge JG, Zhang L et al. Laser powder bed fusion of NiTiFe shape memory alloy via pre-mixed powder: microstructural evolution, mechanical and functional properties. *Rare Met*, 2024; 43: 2300-2316.[DOI]

[50] Guo C, Yuan B, Du P et al. Laser beam powder bed fusion of NiTiFe shape memory alloys by in-situ alloying: microstructural evolution and generation of strain glass. *Virtual Phys Prototyp*, 2025; 20: e2438896.[DOI]

[51] Biasutti T, Bettini P, Nespoli A et al. 3D printing of shape memory alloys for complex architectures of smart structures. *Acta Astronaut*, 2024; 221: 206-217.[DOI]

[52] Vilella T, Rodríguez D, Fargas G. Additive manufacturing of Ni-free Ti-based shape memory alloys: A review. *Biomater Adv*, 2024; 158: 213774.[DOI]

[53] Huang Y, Xin D, Chen X. Microstructure and properties of NiTi shape memory alloy fabricated by double-wire plasma arc additive manufacturing with a nearly equal atomic ratio. *Mater Lett*, 2024; 354: 135406.[DOI]

[54] Khoo ZX, Liu Y, An J et al. A review of selective laser melted NiTi shape memory alloy. *Materials*, 2018; 11: 519.[DOI]

[55] Wang X, Yu J, Liu J et al. Effect of process parameters on the phase transformation behavior and tensile properties of NiTi shape memory alloys fabricated by selective laser melting. *Addit Manuf*, 2020; 36: 101545.[DOI]

[56] Zhang Q, Hao S, Liu Y et al. The microstructure of a selective laser melting (SLM)-fabricated NiTi shape memory alloy with superior tensile property and shape memory recoverability. *Appl Mater Today*, 2020; 19: 100547.[DOI]

[57] Ford S, Despeisse M. Additive manufacturing and sustainability: an exploratory study of the advantages and challenges. *J Clean Prod*, 2016; 137: 1573-1587.[DOI]

[58] Izadi M, Farzaneh A, Mohammed M et al. A review of laser engineered net shaping (LENS) build and process parameters of metallic parts. *Rapid Prototyping J*, 2020; 26: 1059-1078.[DOI]

[59] Wang X, Kustov S, Van Humbeeck J. A short review on the microstructure, transformation behavior and functional properties of NiTi shape memory alloys fabricated by selective laser melting. *Materials*, 2018; 11: 1683.[DOI]

[60] Saedi S, Saghaian SE, Jahadakbar A et al. Shape memory response of porous NiTi shape memory alloys fabricated by selective laser melting. *J Mater Sci Mater Med*, 2018; 29: 40.[DOI]

[61] Zhang C, Zhu J, Zheng H et al. A review on microstructures and properties of high entropy alloys manufactured by selective laser melting. Int *J Extreme Manuf*, 2020; 2: 032003.[DOI]

[62] Wei S, Song B, Zhang Y et al. Mechanical response of triply periodic minimal surface structures manufactured by selective laser melting with composite materials. *Acta Metall Sin (Engl Lett)*, 2022; 35: 397-410.[DOI]

[63] Chen W, Yang Q, Huang S et al. Laser power modulated

microstructure evolution, phase transformation and mechanical properties in NiTi fabricated by laser powder bed fusion. *J Alloys Compd*, 2021; 861: 157959.[DOI]

[64] Guo W, Sun Z, Yang Y et al. Study on the junction zone of NiTi shape memory alloy produced by selective laser melting via a stripe scanning strategy. *Intermetallics*, 2020; 126: 106947.[DOI]

[65] Hsu TY. Fe-Mn-Si based shape memory alloys. *Mater Sci Forum*, 2000; 327: 199-206.[DOI]

[66] Wang C, Tan XP, Du Z et al. Additive manufacturing of NiTi shape memory alloys using pre-mixed powders. *J Mater Process Technol*, 2019; 271: 152-161.[DOI]

[67] Behera A. Smart applications of NiTi shape memory alloy in biomedical industries. In: Nickel-Titanium Smart Hybrid Materials. Elsevier, 2022: 327-354.[DOI]

[68] Sharma N, Raj T, Jangra K. Applications of nickel-titanium alloy. *J Eng Technol*, 2015; 5: 1-11.[DOI]

[69] Farber E, Zhu JN, Popovich A et al. A review of NiTi shape memory alloy as a smart material produced by additive manufacturing. *Mater Today Proc*, 2020; 30: 761-767.[DOI]

[70] Bourell DL, Beaman JJ, Wohlers T. History and evolution of additive manufacturing. In: Additive Manufacturing Processes. *ASM International*, 2020: 11-18.[DOI]

[71] Dzogbewu TC. Laser powder bed fusion of Ti15Mo. *Results Eng*, 2020; 7: 100155.[DOI]

[72] Ramosena LA, Dzogbewu TC, du Preez W. Direct metal laser sintering of the Ti6Al4V alloy from a powder blend. *Materials*, 2022; 15: 8193.[DOI]

[73] Singh R, Gupta A, Tripathi O et al. Powder bed fusion process in additive manufacturing: An overview. *Mater Today Proc*, 2020; 26: 3058-3070.[DOI]

[74] Kok Y, Tan XP, Wang P et al. Anisotropy and heterogeneity of microstructure and mechanical properties in metal additive manufacturing: A critical review. *Mater Des*, 2018; 139: 565-586.[DOI]

[75] Lindhe U, Harrysson O. Rapid manufacturing with electron beam melting (EBM) - a manufacturing revolution. 2003.

[76] Li B, Wang L, Wang B et al. Solidification characterization and its correlation with the mechanical properties and functional response of NiTi shape memory alloy manufactured by electron beam freeform fabrication. *Addit Manuf*, 2021; 48: 102468.[DOI]

[77] Li B, Wang L, Wang B et al. Electron beam freeform fabrication of NiTi shape memory alloys: crystallography, martensitic transformation, and functional response. *Mater Sci Eng A*, 2022; 843: 143135.[DOI]

[78] Naderifar M, Goli H, Ghaljaie F. Snowball sampling: A purposeful method of sampling in qualitative research. *Strides Dev Med Educ*, 2017; 14: 1-6.[DOI]

[79] Dzogbewu TC, de Beer DJ. Additive manufacturing of NiTi shape memory alloy and its industrial applications. *Heliyon*, 2024; 10: e23369.[DOI]

[80] Alaneme KK, Okotete EA. Reconciling viability and cost-effective shape memory alloy options - A review of copper and iron based shape memory metallic systems. *Eng Sci Technol Int J*, 2016; 19: 1582-1592.[DOI]

[81] Otsuka K, Shimizu K. Pseudoelasticity and shape memory effects in alloys. *Int Met Rev*, 1986; 31: 93-114.[DOI]

[82] Kheirikhah MM, Rabiee S, Edalat ME. A review of shape memory alloy actuators in robotics. A Review of Shape Memory Alloy Actuators in Robotics. In: Ruiz-del-Solar J, Chown E, Plöger PG (eds). RoboCup 2010: Robot Soccer World Cup XIV (RoboCup 2010). Lecture Notes in Computer Science ((LNAI,volume 6556)), Springer, Berlin, Heidelberg. 2011: 206-217.[DOI]

[83] Foudzi FM, Jamhari FI, Sulong AB et al. 4D printing of shape memory alloy with selective laser melting (SLM): A brief review. In: International Conference on Advancement in Materials, Manufacturing and Energy Engineering. Springer, 2024: 241-246.[DOI]

[84] Yang Q, Sun K, Yang C et al. Compression and superelasticity behaviors of NiTi porous structures with tiny strut fabricated by selective laser melting. *J Alloys Compd*, 2021; 858: 157674.[DOI]

[85] Yu Z, Xu Z, Guo Y et al. Analysis of microstructure, mechanical properties, wear characteristics and corrosion behavior of SLM-NiTi under different process parameters. *J Manuf Processes*, 2022; 75: 637-650.[DOI]

[86] Khoo ZX, An J, Chua CK et al. Effect of heat treatment on repetitively scanned SLM NiTi shape memory alloy. *Materials*, 2018; 12: 77.[DOI]

[87] Feng B, Wang C, Zhang Q et al. Effect of laser hatch spacing on the pore defects, phase transformation and properties of selective laser melting fabricated NiTi shape memory alloys. *Mater Sci Eng A*, 2022; 840: 142965.[DOI]

[88] Zhao C, Liang H, Luo S et al. The effect of energy input on reaction, phase transition and shape memory effect of NiTi alloy by selective laser melting. *J Alloys Compd*, 2020; 817: 153288.[DOI]

[89] Liu M, Zhu JN, Popovich VA et al. Passive film formation and corrosion resistance of laser-powder bed fusion fabricated NiTi shape memory alloys. *J Mater Res Technol*, 2023; 23: 2991-3006.[DOI]

[90] Guo F, Guo Y, Kong X et al. The effect of wall thickness and scanning speed on the martensitic transformation and tensile properties of selective laser melted NiTi thin-wall structures. *Metals*, 2022; 12: 519.[DOI]

[91] Ma G, Hu Y, Zhang L et al. Phase transformation behavior and mechanical properties of NiTi shape memory alloys fabricated by directed laser deposition. *Mater Sci Eng A*, 2024; 908: 146693.[DOI]

[92] Ge J, Liu H, Yuan B et al. Selective laser melting of the ternary NiTi+3Cu shape memory alloys with excellent properties via microstructural tailoring. *J Alloys Compd*, 2024; 1002: 175395.[DOI]

[93] Lu J, Zhang C, Liu Y et al. NiTi alloys with simultaneous equiaxed-grain strength and columnar-grain ductility manipulated by direct energy deposition. *J Alloys Compd*, 2025; 1010: 180601.[DOI]

[94] Lu HZ, Yang C, Luo X et al. Ultrahigh-performance TiNi shape memory alloy by 4D printing. *Mater Sci Eng A*, 2019; 763: 138166.[DOI]

[95] Băbțan AM, Timuș D, Sorițău O et al. Tissue integration and biological cellular response of SLM-manufactured titanium scaffolds. *Metals*, 2020; 10: 1192.[DOI]

[96] Ratajski J, Bałasz B, Mydłowska K et al. The effect of ageing on phase transformations and mechanical behaviour in Ni-rich NiTi alloys. *Materials*, 2024; 17: 2420.[DOI]

[97] Gu Q, Li H, Yang Z et al. Microstructure and phase transformation temperature of NiTiNb shape memory alloy prepared by laser solid forming using mixed powder. *Appl Sci*, 2022; 12: 2371.[DOI]

[98] Chmielewska A, Wysocki B, Kwaśniak P et al. Heat treatment of NiTi alloys fabricated using laser powder bed fusion (LPBF) from elementally blended powders. *Materials*, 2022; 15: 3304.[DOI]

[99] Yang J, Zhao C, Liang H et al. Spinodal decomposition and martensitic transformation of the high manganese Mn–xCu alloys fabricated by additive manufacturing. *Appl Mater Today*, 2021; 25: 101170.[DOI]

[100] Liu J, Deng Y, Guo X. Study the correlation of B19‘ phase transformation and grain orientation evolution on shape recovery of NiTi alloys fabricated by powder bed fusion. *Mater Charact*, 2023; 205: 113297.[DOI]

[101] Chang SH, Liao BS, Gholami-Kermanshahi M. Effect of Co additions on the damping properties of Cu-Al-Ni shape memory alloys. *J Alloys Compd*, 2020; 847: 156560.[DOI]

[102] Shafeeq MM, Hirshikesh, Gupta GK et al. Influence of Mn on the

mechanical and shape memory transformation behaviours of powder metallurgy processed Cu-Al-Ni SMAs. *Met Mater Int*, 2024; 30: 211-219.[DOI]

[103] Agrawal A, Dube RK. Methods of fabricating Cu-Al-Ni shape memory alloys. *J Alloys Compd*, 2018; 750: 235-247.[DOI]

[104] Chang SH. Influence of chemical composition on the damping characteristics of Cu-Al-Ni shape memory alloys. *Mater Chem Phys*, 2011; 125: 358-363.[DOI]

[105] Saud SN, Hamzah E, Abubakar T et al. Effect of a fourth alloying element on the microstructure and mechanical properties of Cu-Al-Ni shape memory alloys. *J Mater Res*, 2015; 30: 2258-2269.[DOI]

[106] Di Cocco V, Iacoviello F, Natali S et al. Fatigue crack behavior on a Cu-Zn-Al SMA. *Fract Struct Integr*, 2014; 8: 454-461.[DOI]

[107] Wu SK, Chan WJ, Chang SH. Damping characteristics of inherent and intrinsic internal friction of Cu-Zn-Al shape memory alloys. *Metals*, 2017; 7: 397.[DOI]

[108] Lokesh N, Shivasiddaramaiah AG, Mallik US et al. Tribological evolution of Cu-Zn-Al shape memory alloys: insights through systematic optimization. *J Inst Eng India Ser D*, 2025; 106: 123-134.[DOI]

[109] Lokesh N, Mallik US, Shivasiddaramaiah AG et al. Synergistic analysis of shape memory behavior, corrosion resistance, and microstructural dynamics in Cu-Zn-Al shape memory alloys across varied environments. *J Inst Eng India Ser D*, 2025; 106: 135-147.[DOI]

[110] Lovey FC, Torra V. Shape memory in Cu-based alloys: phenomenological behavior at the mesoscale level and interaction of martensitic transformation with structural defects in Cu-Zn-Al. *Prog Mater Sci*, 1999; 44: 189-289.[DOI]

[111] Mallik US, Sampath V. Influence of aluminum and manganese concentration on the shape memory characteristics of Cu–Al–Mn shape memory alloys. *J Alloys Compd*, 2008; 459: 142-147.[DOI]

[112] Qiu CX, Zhu S. Characterization of cyclic properties of superelastic monocrystalline Cu-Al-Be SMA wires for seismic applications. *Constr Build Mater*, 2014; 72: 219-230.[DOI]

[113] Naresh H, Prashantha S, Santhosh N. Mechanical, fatigue and super plasticity properties of Cu-Al-Mn, Cu-Al-Be-Mn shape memory alloy and their metal matrix composites. *RSC Adv*, 2024; 14: 31275-31290.[DOI]

[114] Singh RK, Biswas P, Murigendrappa SM et al. An experimental evaluation of the microstructure, mechanical and functional fatigue properties of the boron-doped Cu-Al-Be SMA wires. *Mater Des*, 2021; 210: 110081.[DOI]

[115] Figueroa CG, Garcia-Castillo FN, Jacobo VH et al. Microstructural and superficial modification in a Cu-Al-Be shape memory alloy due to superficial severe plastic deformation under sliding wear conditions. *IOP Conf Ser Mater Sci Eng*, 2017; 194: 012011.[DOI]

[116] Benlachemi R, Ogam E, Ongwen N et al. Investigating the Young's modulus of Cu-Al-Be shape memory alloy using a phase diagram, vibration spectroscopy and ultrasonic waves. *J Alloys Compd*, 2024; 976: 173010.[DOI]

[117] Lopez-Ferreño I, Breczewski T, Ruiz-Larrea I et al. Thermal treatments and transformation behavior of Cu-Al-Be shape memory alloys. *J Alloys Compd*, 2013; 577: S463-S467.[DOI]

[118] Sutou Y, Omori T, Wang JJ et al. Characteristics of Cu-Al-Mn-based shape memory alloys and their applications. *Mater Sci Eng A*, 2004; 378: 278-282.[DOI]

[119] Sutou Y, Omori T, Kainuma R et al. Ductile Cu-Al-Mn based shape memory alloys: general properties and applications. *Mater Sci Technol*, 2008; 24: 896-901.[DOI]

[120] Milosavljevic D, Bassani P, Cinquemani S et al. Effects of thermomechanical treatments on Cu-Al-Mn shape memory alloys. *Mater Chem Phys*, 2023; 302: 127756.[DOI]

[121] Araki Y, Endo T, Omori T et al. Potential of superelastic Cu-Al-Mn alloy bars for seismic applications. *Earthq Eng Struct Dyn*, 2011; 40: 107-115.[DOI]

[122] Koeda N, Omori T, Sutou Y et al. Damping properties of ductile Cu-Al-Mn-based shape memory alloys. *Mater Trans*, 2005; 46: 118-122.[DOI]

[123] Peltier L, Perroud O, Moll P et al. Production and mechanical properties of Cu-Al-Ni-Be shape memory alloy thin ribbons using a cold co-rolled process. *Shape Mem Superelasticity*, 2021; 7: 344-352.[DOI]

[124] Ehrmann G, Ehrmann A. 3D printing of shape memory polymers. *J Appl Polym Sci*, 2021; 138: 50847.[DOI]

[125] Prakash A, Arunav H, Vishnu J et al. Emergence of Copper-Based Shape Memory Alloys for Robotics Applications: From Past To Present. *Met Mater Int*, 2025; 31: 1199-1241.[DOI]

[126] Singh S, Palani IA, Dehghahi S et al. Development of Cu-based shape memory alloy through selective laser melting from elemental powder mixture: Processing and characterization. *J Alloys Compd*, 2023; 961: 171029.[DOI]

[127] Jia H, Sun H, Wang H et al. Scanning strategy in selective laser melting (SLM): a review. *Int J Adv Manuf Technol*, 2021; 113: 2413-2435.[DOI]

[128] Gao B, Zhao H, Peng L et al. A review of research progress in selective laser melting (SLM). *Micromachines*, 2022; 14: 57.[DOI]

[129] Mansoura A, Omidi N, Barka N et al. Selective laser melting of stainless steels: a review of process, microstructure and properties. *Met Mater Int*, 2024; 30: 2343-2371.[DOI]

[130] Agius D, Kourousis KI, Wallbrink C. A review of the as-built SLM Ti-6Al-4V mechanical properties towards achieving fatigue resistant designs. *Metals*, 2018; 8: 75.[DOI]

[131] Jalali M, Mohammadi K, Movahhedy MR et al. SLM additive manufacturing of NiTi porous implants: a review of constitutive models, finite element simulations, manufacturing, heat treatment, mechanical, and biomedical studies. *Met Mater Int*, 2023; 29: 2458-2491.[DOI]

[132] Haleem AH, Khulief ZT, Kadhim IN. Modification of corrosion and mechanical behaviour of Cu-Zn-Al shape memory alloy. *J Phys Conf Ser*, 2021; 1973: 012049.[DOI]

[133] Mohan M, Krishna TV, Rao DJ et al. Influence of silver addition on wear characteristics of Cu-Al-Mn shape memory alloys. *Mater Today Proc*, 2023.[DOI]

[134] Liverić L, Holjevac Grgurić T, Mandić V et al. Influence of manganese content on martensitic transformation of Cu-Al-Mn-Ag alloy. *Materials*, 2023; 16: 5782.[DOI]

[135] Qian S, Geng Y, Wang Y et al. Elastocaloric effect in CuAlZn and CuAlMn shape memory alloys under compression. *Philos Trans R Soc A*, 2016; 374: 20150309.[DOI]

[136] Dutta S, Singh AK, Paul B et al. Machining of shape-memory alloys using electrical discharge machining with an elaborate study of optimization approaches: a review. *J Braz Soc Mech Sci Eng*, 2022; 44: 557.[DOI]

[137] Karthik M, Abhinav J, Shankar KV. Morphological and mechanical behaviour of Cu-Sn alloys - a review. *Met Mater Int*, 2021; 27: 1915-1946.[DOI]

[138] Dang M, Xiang H, Li J et al. Laser powder bed fusion of full martensite Cu-Al-Mn-Ti alloy with good superelasticity and shape memory effect. *Mater Sci Eng A*, 2023; 884: 145475.[DOI]

[139] da Silva MR, Gargarella P, Gustmann T et al. Laser surface remelting of a Cu-Al-Ni-Mn shape memory alloy. *Mater Sci Eng A*, 2016; 661: 61-67.[DOI]

[140] Mohamed OA, Masood SH, Xu W. Nickel-titanium shape memory alloys made by selective laser melting: a review on process optimisation. *Adv Manuf*, 2022; 10: 24-58.[DOI]

[141] Saud SN, Hamzah E, Abubakar T et al. Effects of Mn additions on the structure, mechanical properties, and corrosion behavior of Cu-Al-Ni shape memory alloys. *J Mater Eng Perform*, 2014; 23: 3620-3629.[DOI]

[142] Tian J, Zhu W, Wei Q et al. Process optimization, microstructures and mechanical properties of a Cu-based shape memory alloy fabricated by selective laser melting. *J Alloys Compd*, 2019; 785: 754-764.[DOI]

[143] Gustmann T, Neves A, Kühn U et al. Influence of processing parameters on the fabrication of a Cu-Al-Ni-Mn shape-memory alloy by selective laser melting. *Addit Manuf*, 2016; 11: 23-31.[DOI]

[144] Abolhasani D, Han SW, VanTyne CJ et al. Enhancing the shape memory effect of Cu-Al-Ni alloys via partial reinforcement by alumina through selective laser melting. *J Mater Res Technol*, 2021; 15: 4032-4047.[DOI]

[145] Gustmann T, Schwab H, Kühn U et al. Selective laser remelting of an additively manufactured Cu-Al-Ni-Mn shape-memory alloy. *Mater Des*, 2018; 153: 129-138.[DOI]

[146] Dennis GEA, Santos J, Kiminami CS et al. Comparison of Cu-Al-Ni-Mn-Zr shape memory alloy prepared by selective laser melting and conventional powder metallurgy. *Trans Nonferrous Met Soc China*, 2020; 30: 3322-3332.[DOI]

[147] Shishkovsky I, Yadroitsev I, Morozov Y. Laser-assisted synthesis in Cu-Al-Ni system and some of its properties. *J Alloys Compd*, 2016; 658: 875-879.[DOI]

[148] Pérez-Cerrato M, Gómez-Cortés JF, Urionabarrenetxea E et al. Optimising the laser powder bed fusion processing parameters of Cu-Al-Ni shape memory alloys: microstructure and functional properties relationship. *Virtual Phys Prototyp*, 2025; 20: e2458679.[DOI]

[149] Babacan N, Pilz S, Hufenbach J et al. Effects of remelting on the properties of a superelastic Cu-Al-Mn shape memory alloy fabricated by laser powder bed fusion. *Shape Mem Superelasticity*, 2023; 9: 447-459.[DOI]

[150] Zhuo L, Song B, Li R et al. Effect of element evaporation on the microstructure and properties of CuZnAl shape memory alloys prepared by selective laser melting. *Opt Laser Technol*, 2020; 127: 106164.[DOI]

[151] He L, Li Y, Su Q et al. Fabrication of Cu-Al-Mn-Ti shape memory alloys via selective laser melting and its nano-precipitation strengthening. *Micromachines*, 2025; 16: 857.[DOI]

[152] Xi X, Zhang J, Tang H et al. The ultrahigh functional response of CuAlMnNb shape memory alloy by selective laser melting. *J Mater Res Technol*, 2022; 20: 671-680.[DOI]

[153] Babacan N, Pauly S, Gustmann T. Laser powder bed fusion of a superelastic Cu-Al-Mn shape memory alloy. *Mater Des*, 2021; 203: 109625.[DOI]

[154] Wu MW, Hu ZF, Yang BB et al. Additive manufacturing of Cu-Al-Mn shape memory alloy with enhanced superelasticity. *Rare Met*, 2023; 42: 4234-4245.[DOI]

[155] Niedbalski S, Durán A, Walczak M et al. Laser-assisted synthesis of Cu-Al-Ni shape memory alloys: Effect of inert gas pressure and Ni content. *Materials*, 2019; 12: 794.[DOI]

[156] Singh S, Narayanan JA, Dehghahi S et al. Revealing the impact of hot isostatic pressing temperature on the microstructure and mechanical characteristics of selective laser melted CuAlNiMn shape memory alloy. *Mater Lett*, 2024; 365: 136452.[DOI]

[157] Felice IO, Shen J, Serrati DM et al. Arc-based additive manufacturing of Cu-Al-Mn shape memory alloys: microstructure, tensile behavior and superelastic properties. *Mater Sci Eng A*, 2026; 957: 149923.[DOI]

[158] Fengqin W, Yinfang J, Dejun K. Microstructure, mechanical properties, and tribological properties of Fe45Mn35Co10Cr10 high-entropy alloy reinforced Cu11.85Al3.2Mn0.1Ti shape memory alloy coatings by laser cladding. *J Mater Eng Perform*, 2025.[DOI]

[159] Zheng D, Li R, Kang J et al. Achieving superelastic shape recoverability in smart flexible CuAlMn metamaterials via 3D printing. *Int J Mach Tools Manuf*, 2024; 195: 104110.[DOI]

[160] Pérez-Cerrato M, Fraile I, Gómez-Cortés JF et al. Designing for shape memory in additive manufacturing of Cu-Al-Ni shape memory alloy processed by laser powder bed fusion. *Materials*, 2022; 15: 6284.[DOI]

[161] Sun Q, Tan X, Ding M et al. A review of additively manufactured iron-based shape memory alloys. *Crystals*, 2024; 14: 773.[DOI]

[162] Kim D, Ferretto I, Leinenbach C et al. 3D and 4D printing of complex structures of Fe-Mn-Si-based shape memory alloy using laser powder bed fusion. *Adv Mater Interfaces*, 2022; 9: 2200171.[DOI]

[163] Niendorf T, Brenne F, Krooß P et al. Microstructural evolution and functional properties of Fe-Mn-Al-Ni shape memory alloy processed by selective laser melting. *Metall Mater Trans A*, 2016; 47: 2569-2573.[DOI]

[164] Yang X, Yin X, He Y et al. Selective laser melted Fe-30Mn-6Cu alloy: A multifunctional candidate for MRI-compatible, biodegradable, antibacterial, and biocompatible orthopedic implants. *Int J Bioprint*, 2025; 11: 358.[DOI]

[165] Wei C, Li L. Recent progress and scientific challenges in multi-material additive manufacturing via laser-based powder bed fusion. *Virtual Phys Prototyp*, 2021; 16: 347-371.[DOI]

[166] Xiong Z, Li H, Yang H et al. Micro laser powder bed fusion of NiTi alloys with superior mechanical property and shape recovery function. *Addit Manuf*, 2022; 57: 102960.[DOI]

[167] Xue L, Atli KC, Zhang C et al. Laser powder bed fusion of defect-free NiTi shape memory alloy parts with superior tensile superelasticity. *Acta Mater*, 2022; 229: 117781.[DOI]

[168] Nematollahi M, Saghaian SE, Safaei K et al. Building orientation-structure-property in laser powder bed fusion of NiTi shape memory alloy. *J Alloys Compd*, 2021; 873: 159791.[DOI]

[169] Liu H, Gu D, Shi K et al. High-strength aluminum alloy processed by micro laser powder bed fusion (μ-LPBF): Coordination of laser formability, microstructure evolution, and mechanical properties. *J Mater Process Technol*, 2024; 332: 118580.[DOI]

[170] Liu H, Gu D, Huang G et al. Underlying role of micro-area energy input mode on formability and performance of high-strength aluminum alloy processed by micro laser powder bed fusion (μ-LPBF). *Addit Manuf*, 2025; 96: 104892.[DOI]

[171] Zhang Y, Gu D, Liu H et al. Improving surface finish of Al-Mg-Sc-Zr alloy by thermodynamics control and process optimization during high-precision micro laser powder bed fusion (μ-LPBF). *Adv Eng Mater*, 2025; 27: 2402702.[DOI]

[172] Zhang T, Wang X, Zhang D et al. Mesoscopic simulation of thermal dynamics in melt pool and melting behavior of individual powder particles during NiTi alloys fabrication by μ-LPBF. *Addit Manuf*, 2025; 96: 104918.[DOI]

[173] Shishkovsky IV. Shape memory effect in porous volume NiTi articles fabricated by selective laser sintering. *Tech Phys Lett*, 2005; 31: 186-188.[DOI]

[174] Shishkovsky IV, Volova LT, Kuznetsov MV et al. Porous biocompatible implants and tissue scaffolds synthesized by selective laser sintering from Ti and NiTi. *J Mater Chem*, 2008; 18: 1309-1317.[DOI]

[175] Pu Z, Du D, Wang K et al. Study on the NiTi shape memory alloys in-situ synthesized by dual-wire-feed electron beam additive manufacturing. *Addit Manuf*, 2022; 56: 102886.[DOI]

[176] Pu Z, Du D, Zhang D et al. Improvement of tensile superelasticity by aging treatment of NiTi shape memory alloys fabricated by electron beam wire-feed additive manufacturing. *J Mater Sci Technol*, 2023; 145: 185-196.[DOI]

[177] Sojoodi M, Behvar A, Bajaj H et al. Integration of circular economy into metal additive manufacturing: A review of ultrasonic plasma atomization for producing virgin and recycled NiTi powder. *Shape Mem Superelasticity*, 2025; 11: 1-41.[DOI]

[178] Mitchell A, Lafont U, Hołyńska M et al. Additive manufacturing - A review of 4D printing and future applications. *Addit Manuf*, 2018; 24: 606-626.[DOI]

[179] Kubášová K, Drátovská V, Losertová M et al. A review on additive manufacturing methods for NiTi shape memory alloy production. *Materials*, 2024; 17: 1248.[DOI]

[180] Sinha A, Rajak DK, Shaik NB et al. A review on 4D printing of nickel-titanium smart alloy processing, the effect of major parameters and their biomedical applications. *Proc Inst Mech Eng E J Process Mech Eng*, 2025; 239: 1616-1625.[DOI]

[181] Singh J, Hashmi AW. Recent progress in shape memory alloys and additive manufacturing. In: Green Technology and Smart Materials for Engineering Applications. Springer, 2025: 48-73.[DOI]

[182] Chen X, Liu K, Guo W et al. The fabrication of NiTi shape memory alloy by selective laser melting: a review. *Rapid Prototyping J*, 2019; 25: 1421-1432.[DOI]

[183] Krooß P, Günther J, Halbauer L et al. Electron beam welding of Fe–Mn–Al–Ni shape memory alloy: microstructure evolution and shape memory response. *Funct Mater Lett*, 2017; 10: 1750043.[DOI]

[184] Varadharajan S, Vasanthan KS, Agarwal P. Application of reversible four-dimensional printing of shape memory alloys and shape memory polymers in structural engineering: A state-of-the-art review. *3D Print Addit Manuf*, 2024; 11: 919-953.[DOI]

[185] Dutkiewicz J, Rogal Ł, Kalita D et al. Microstructure, mechanical properties, and martensitic transformation in NiTi shape memory alloy fabricated using electron beam additive manufacturing technique. *J Mater Eng Perform*, 2022; 31: 1609-1621.[DOI]

[186] Otubo J, Rigo OD, Neto CM et al. The effects of vacuum induction melting and electron beam melting techniques on the purity of NiTi shape memory alloys. *Mater Sci Eng A*, 2006; 438: 679-682.[DOI]

[187] Altug-Peduk GS, Dilibal S, Harrysson O et al. Experimental investigation on the EBM-based additively manufactured prismatic nickel-titanium SMA components. *Russ J Non-Ferrous Met*, 2021; 62: 357-367.[DOI]

[188] Ma S, Li Y, Kan W et al. Enhancement of grain refinement and heat resistance in TiB2-reinforced Al-Cu-Mg-Fe-Ni matrix composite additive manufactured by electron beam melting. *J Alloys Compd*, 2022; 924: 166395.[DOI]

[189] Sharabian E, Leary M, Fraser D et al. Electron beam powder bed fusion of copper components: A review of mechanical properties and research opportunities. *Int J Adv Manuf Technol*, 2022; 122: 513-532.[DOI]

[190] Khoroshko ES, Filippov AV, Shamarin NN et al. Structure and mechanical properties of Cu-Al-Si-Mn system-based copper alloy obtained by additive manufacturing. *Russ Phys J*, 2021; 64: 333-339.[DOI]

[191] Momeni S, Guschlbauer R, Osmanlic F et al. Selective electron melting of a copper-chrome powder mixture. *Mater Lett*, 2018; 223: 250-252.[DOI]

[192] Ramirez DA, Murr LE, Li SJ et al. Open-cellular copper structures fabricated by additive manufacturing using electron beam melting. *Mater Sci Eng A*, 2011; 528: 5379-5386.[DOI]

[193] Sanchez JC, Murr LE, Staudhammer KP. Effect of grain size and pressure on twinning and microbanding in oblique shock loading of copper rods. *Acta Mater*, 1997; 45: 3223-3235.[DOI]

[194] Wen S, Tan Y, Shi S et al. Thermal contact resistance between the surfaces of silicon and copper crucible during electron beam melting. *Int J Therm Sci*, 2013; 74: 37-43.[DOI]

[195] Calleja-Ochoa A, Gonzalez-Barrio H, Lopez de Lacalle N et al. A new approach in the design of microstructured ultralight components to achieve maximum functional performance. *Materials*, 2021; 14: 1588.[DOI]

[196] Wolf T, Fu Z, Ye J et al. Periodic open cellular Raney-copper catalysts fabricated via selective electron beam melting. *Adv Eng Mater*, 2020; 22: 1901524.[DOI]

[197] Hussain A, Khan A, Khan MI et al. In-depth analysis of TiNiPdCu high-temperature shape memory alloys synthesized using powder metallurgy technique. *Eng Rep*, 2025; 7: e70245.[DOI]

[198] Gamzina D, Luhmann NC, Ledford C et al. Additive vacuum electronics: Electron beam melting of copper. In: 2017 Eighteenth International Vacuum Electronics Conference (IVEC). *IEEE*, 2017: 1-2.[DOI]

[199] Bauer A, Wiegand M, Wicke P et al. Electron beam welding of hot-rolled Fe-Mn-Al-Ni shape memory alloy sheets. *Shape Mem Superelasticity*, 2023; 9: 364-376.[DOI]

[200] Torrent C, Bauer A, Vollmer M et al. On the challenges toward realization of functionally graded structures by electron beam melting—Fe-base shape memory alloy and stainless steel. In: Structural Integrity of Additive Manufactured Materials and Parts. *ASTM International*, 2020: 20-33.[DOI]

[201] Yu L, Chen K, Zhang Y et al. Microstructures and mechanical properties of NiTi shape memory alloys fabricated by wire arc additive manufacturing. *J Alloys Compd*, 2022; 892: 162193.[DOI]

[202] Treutler K, Wesling V. The current state of research of wire arc additive manufacturing (WAAM): a review. *Appl Sci*, 2021; 11: 8619.[DOI]

[203] Meena RP, N Y, Vipin. A review on wire arc additive manufacturing based on cold metal transfer. *Mater Manuf Processes*, 2024; 39: 1315-1341.[DOI]

[204] Goswami T, Biswas S, Das S et al. An overview of wire arc additive manufacturing (WAAM) technique with different alloys in modern manufacturing industries. In: Hybrid Metal Additive Manufacturing. Woodhead Publishing: Cambridge, UK, 2023: 19-29.[DOI]

[205] Sha G, Cerezo A. Early-stage precipitation in Al-Zn-Mg-Cu alloy (7050). *Acta Mater*, 2004; 52: 4503-4516.[DOI]

[206] Pant H, Arora A, Gopakumar GS et al. Applications of wire arc additive manufacturing (WAAM) for aerospace component manufacturing. *Int J Adv Manuf Technol*, 2023; 127: 4995-5011.[DOI]

[207] Çam G. Prospects of producing aluminum parts by wire arc additive manufacturing (WAAM). *Mater Today Proc*, 2022; 62: 77-85.[DOI]

[208] Singh SR, Khanna P. Wire arc additive manufacturing (WAAM): A new process to shape engineering materials. *Mater Today Proc*, 2021; 44: 118-128.[DOI]

[209] Xia C, Pan Z, Polden J et al. A review on wire arc additive manufacturing: Monitoring, control and a framework of automated system. *J Manuf Syst*, 2020; 57: 31-45.[DOI]

[210] Thapliyal S. Challenges associated with the wire arc additive manufacturing (WAAM) of aluminum alloys. *Mater Res Express*, 2019; 6: 112006.[DOI]

[211] Xu M, Chen S, Yuan T et al. Effect of thermal cycles on the microstructure and properties of the Al-Zn-Mg-Cu alloy during wire-arc additive manufacturing. *J Alloys Compd*, 2022; 928: 167172.[DOI]

[212] Xu M, Zhang H, Yuan T et al. Microstructural characteristics and cracking mechanism of Al-Cu alloys in wire arc additive manufacturing. *Mater Charact*, 2023; 197: 112677.[DOI]

[213] Li K, Yang T, Hou X et al. Microstructure evolution and mechanical properties of Al-Cu-Mn-Cd alloy fabricated by CMT-wire arc additive manufacturing. *Mater Sci Eng A*, 2024; 898: 146395.[DOI]

[214] Li T, Wang Z, Hu S et al. Hot cracking during the fabrication of

Inconel 625/stainless steel 308 L functionally graded material by dual-wire arc additive manufacturing. *J Manuf Processes*, 2022; 82: 461-473.[DOI]

[215] Koley S, Ganguly S. Prevention of hot cracking in wire-arc additive manufacturing of iron-based shape memory alloy using a novel inter-layer machine hammer peening process. *Mater Sci Eng A*, 2025; 937: 148453.[DOI]

[216] Felice IO, Shen J, Barragan AF et al. Wire and arc additive manufacturing of Fe-based shape memory alloys: microstructure, mechanical and functional behavior. *Mater Des*, 2023; 231: 112004.[DOI]

[217] Haberland C, Elahinia M, Walker JM et al. On the development of high quality NiTi shape memory and pseudoelastic parts by additive manufacturing. Smart *Mater Struct*, 2014; 23: 104002.[DOI]

[218] ASTM F2063. Standard Specification for Wrought Nickel-Titanium Shape Memory Alloys for Medical Devices and Surgical Implants. *ASTM International*, 2000.[DOI]

[219] Tan C, Li S, Essa K et al. Laser powder bed fusion of Ti-rich TiNi lattice structures: Process optimisation, geometrical integrity, and phase transformations. *Int J Mach Tools Manuf*, 2019; 141: 19-29.[DOI]

[220] Hanlon JE, Butler SR, Wasilewski RJ. Effect of martensitic transformation on the electrical and magnetic properties of NiTi. *Trans AIME*, 1967; 239: 1323-1326.

[221] Speirs M, Van Hooreweder B, Van Humbeeck J et al. Fatigue behaviour of NiTi shape memory alloy scaffolds produced by SLM, a unit cell design comparison. *J Mech Behav Biomed Mater,* 2017; 70: 53-59.[DOI]

[222] Habijan T, Haberland C, Meier H et al. The biocompatibility of dense and porous nickel-titanium produced by selective laser melting. *Mater Sci Eng C*, 2013; 33: 419-426.[DOI]

[223] Gustmann T, Gutmann F, Wenz F et al. Properties of a superelastic NiTi shape memory alloy using laser powder bed fusion and adaptive scanning strategies. Prog *Addit Manuf*, 2020; 5: 11-18.[DOI]

[224] Biffi CA, Soyarslan C, Fiocchi J et al. Additive manufacturing of NiTi architected metamaterials. *Addit Manuf Lett*, 2024; 10: 100216.[DOI]

[225] Biffi CA, Bassani P, Fiocchi J et al. Microstructural and mechanical response of NiTi lattice 3D structure produced by selective laser melting. *Metals*, 2020; 10: 814.[DOI]

[226] Lu HZ, Ma HW, Luo X et al. Microstructure, shape memory properties, and in vitro biocompatibility of porous NiTi scaffolds fabricated via selective laser melting. *J Mater Res Technol*, 2021; 15: 6797-6812.[DOI]

[227] Dadbakhsh S, Speirs M, Kruth JP et al. Influence of SLM on shape memory and compression behaviour of NiTi scaffolds. *CIRP Ann*, 2015; 64: 209-212.[DOI]

[228] Chmielewska A, Jahadakbar A, Wysocki B et al. Chemical polishing of additively manufactured, porous, nickel-titanium skeletal fixation plates. 3D Print *Addit Manuf*, 2022; 9: 269-277.[DOI]

[229] Nespoli A, Grande AM, Passaretti F et al. Damping property of a NiTi auxetic structure fabricated through selective laser melting. *Int J Adv Manuf Technol*, 2023; 126: 519-530.[DOI]

[230] Zhang W, Li Z, Xu C et al. Surface characteristics of NiTi cardiovascular stents by selective laser melting and electrochemical polishing. *Int J Adv Manuf Technol*, 2024; 130: 623-634.[DOI]

[231] Hamann I, Gebhardt F, Eisenhut M et al. Investigation into the hybrid production of a superelastic shape memory alloy with additively manufactured structures for medical implants. *Materials*, 2021; 14: 3098.[DOI]

[232] Jahadakbar A, Nematollahi M, Safaei K et al. Design, modeling, additive manufacturing, and polishing of stiffness-modulated porous nitinol bone fixation plates followed by thermomechanical and composition analysis. *Metals*, 2020; 10: 151.[DOI]

[233] Jahadakbar A, Shayesteh Moghaddam N, Amerinatanzi A et al. Finite element simulation and additive manufacturing of stiffness-matched niti fixation hardware for mandibular reconstruction surgery. *Bioengineering*, 2016; 3: 36.[DOI]

[234] Santos CMLD, Cunha FLD, Dynnikov VI. The application of shape memory actuators in anthropomorphic upper limb prostheses. *Artif Organs*, 2003; 27: 473-477.[DOI]

[235] Vincent M, Xolin P, Gevrey AM et al. Experimental and numerical analysis of penetration/removal response of endodontic instrument made of single crystal Cu-based SMA: comparison with NiTi SMA instruments. Smart *Mater Struct*, 2017; 26: 045014.[DOI]

[236] Xolin P, Collard C, Engels-Deutsch M et al. Finite element and experimental structural analysis of endodontic rotary file made of Cu-based single crystal SMA considering a micromechanical behavior model. *Int J Solids Struct*, 2021; 221: 180-196.[DOI]

[237] Demir AG, Previtali B. Additive manufacturing of cardiovascular CoCr stents by selective laser melting. *Mater Des*, 2017; 119: 338-350.[DOI]

[238] Lazic MM, Trišić D, Jakšić M et al. Biocompatibility of copper-based shape memory alloy. *Int Dent J*, 2021; 71: S50.[DOI]

[239] Santosh S, Harris WJ, Srivatsan TS. Environment-induced degradation of shape memory alloys: Role of alloying and nature of environment. *Materials*, 2023; 16: 5660.[DOI]

[240] Zou F, Ma S, Jiang Y et al. Research progress on performance regulation and application of Ti-Ni-based, Fe-based, and Cu-based shape memory alloys. *Adv Eng Res: Possibilities Chall*, 2025; 1: 17-24.[DOI]

[241] Shivasiddaramaiah AG, Mallikarjun US, Praveen N et al. Evaluation of biocompatibility of Cu-Al-Be-Mn quaternary shape memory alloy. *Mater Today Proc*, 2018; 5: 24799-24808.[DOI]

[242] Lazić MM, Lazić M, Milašin J et al. In vitro evaluation of the potential anticancer properties of Cu-based shape memory alloys. *Materials*, 2023; 16: 2851.[DOI]

[243] Li HF, Qiu KJ, Zhou FY et al. Design and development of novel antibacterial Ti-Ni-Cu shape memory alloys for biomedical application. *Sci Rep*, 2016; 6: 37475.[DOI]

[244] Sima Y, Wang W, Abu-Tahon MA et al. An overview of 3D-printed shape memory alloys and applications in biomedical engineering. *Adv Compos Hybrid Mater*, 2024; 7: 148.[DOI]

[245] Srivastava S, Bhalla S, Madan A. Shape memory alloy actuation of non-bonded piezo sensor configuration for bone diagnosis and impedance based analysis. *Biomed Eng Lett*, 2019; 9: 435-447.[DOI]

[246] Aldırmaz E, Tataroğlu A, Dere A et al. Cu-Al-Mn shape memory alloy based Schottky diode formed on Si. *Physica B*, 2019; 560: 261-266.[DOI]

[247] Jani JM, Leary M, Subic A et al. A review of shape memory alloy research, applications and opportunities. *Mater Des*, 2014; 56: 1078-1113.[DOI]

[248] Jayachandran S, Akash K, Prabu SM et al. Investigations on performance viability of NiTi, NiTiCu, CuAlNi and CuAlNiMn shape memory alloy/Kapton composite thin film for actuator application. *Composites Part B*, 2019; 176: 107182.[DOI]

[249] Ishida A, Sato M. Development of polyimide/SMA thin-film actuator. *Mater Sci Forum*, 2010; 654: 2075-2078.[DOI]

[250] Muralidharan M, Jayachandran S, Yogeshwaran M et al. Thermo-mechanical and control behaviour of copper-based shape memory alloy bimorph actuator towards the development of micro positioning system. *Def Sci J*, 2020; 70: 664-671.[DOI]

[251] Reynaerts D, Van Brussel H. A SMA high performance actuator for robot hands. *J Phys IV*, 1991; 1: C4-157.[DOI]

[252] Wongweerayoot E, Srituravanich W, Pimpin A. Fabrication and characterization of nitinol-copper shape memory alloy bimorph actuators. *J Mater Eng Perform*, 2015; 24: 635-643.[DOI]

[253] Ma C, Huang K, Wang C et al. Effect of heat treatment on microstructure and damping properties of MnCu-based damping alloy prepared by laser powder-bed-fusion (LPBF). *Mater Sci Eng A*, 2025; 927: 148050.[DOI]

[254] Hollkamp JP, Scott-Emuakpor O, Celli D. Analyses of damping sustainability of additively manufactured nickel alloy components subjected to high strain loading cycles. In: Turbo Expo 2022. *ASME*, 2022; 86069: V08AT23A003.[DOI]

[255] Scott-Emuakpor O, Beck J, Runyon B et al. Determining unfused powder threshold for optimal inherent damping with additive manufacturing. *Addit Manuf*, 2021; 38: 101739.[DOI]

[256] Germano G, Qaderi S, Adinolfi V et al. Design and modeling of an in-house-built shake table setup for testing prototypes of innovative seismic isolators. *Int J*, 2023; 40: 1-18.

[257] Alaneme KK, Okotete EA, Anaele JU. Structural vibration mitigation - a concise review of the capabilities and applications of Cu and Fe based shape memory alloys in civil structures. *J Build Eng*, 2019; 22: 22-32.[DOI]

[258] Pareek S, Suzuki Y, Araki Y et al. Plastic hinge relocation in reinforced concrete beams using Cu-Al-Mn SMA bars. *Eng Struct*, 2018; 175: 765-775.[DOI]

[259] Araki Y, Kimura K, Asai T et al. Integrated mechanical and material design of quasi-zero-stiffness vibration isolator with superelastic Cu-Al-Mn shape memory alloy bars. *J Sound Vib*, 2015; 358: 74-83.[DOI]